

NRC Publications Archive Archives des publications du CNRC

Cavitation performance testing of podded propellers with different hub taper angle

Islam, M.; He, M.

For the publisher's version, please access the DOI link below./ Pour consulter la version de l'éditeur, utilisez le lien DOI ci-dessous.

Publisher's version / Version de l'éditeur:

<https://doi.org/10.4224/8894908>

Technical Report (National Research Council of Canada. Institute for Ocean Technology); no. TR-2007-04, 2007

NRC Publications Archive Record / Notice des Archives des publications du CNRC :

<https://nrc-publications.canada.ca/eng/view/object/?id=2b24ad42-3975-4ff1-9e62-12fe8fba87c8>

<https://publications-cnrc.canada.ca/fra/voir/objet/?id=2b24ad42-3975-4ff1-9e62-12fe8fba87c8>

Access and use of this website and the material on it are subject to the Terms and Conditions set forth at

<https://nrc-publications.canada.ca/eng/copyright>

READ THESE TERMS AND CONDITIONS CAREFULLY BEFORE USING THIS WEBSITE.

L'accès à ce site Web et l'utilisation de son contenu sont assujettis aux conditions présentées dans le site

<https://publications-cnrc.canada.ca/fra/droits>

LISEZ CES CONDITIONS ATTENTIVEMENT AVANT D'UTILISER CE SITE WEB.

Questions? Contact the NRC Publications Archive team at

PublicationsArchive-ArchivesPublications@nrc-cnrc.gc.ca. If you wish to email the authors directly, please see the first page of the publication for their contact information.

Vous avez des questions? Nous pouvons vous aider. Pour communiquer directement avec un auteur, consultez la première page de la revue dans laquelle son article a été publié afin de trouver ses coordonnées. Si vous n'arrivez pas à les repérer, communiquez avec nous à PublicationsArchive-ArchivesPublications@nrc-cnrc.gc.ca.

DOCUMENTATION PAGE

REPORT NUMBER TR-2007-04	NRC REPORT NUMBER	DATE February 2007	
REPORT SECURITY CLASSIFICATION Unclassified		DISTRIBUTION Unlimited	
TITLE CAVITATION PERFORMANCE TESTING OF PODDED PROPELLERS WITH DIFFERENT HUB-TAPER ANGLES			
AUTHOR(S) Mohammed Fakhru Islam and Moqin He			
CORPORATE AUTHOR(S)/PERFORMING AGENCY(S) Memorial University of Newfoundland Institute for Ocean Technology, National Research Council, St. John's, NL			
PUBLICATION			
SPONSORING AGENCY(S) Memorial University of Newfoundland Institute for Ocean Technology, National Research Council, St. John's, NL			
IOT PROJECT NUMBER		NRC FILE NUMBER	
KEY WORDS Podded, propellers, propulsion, cavitation	PAGES vii, 57, App. A-B	FIGS. 36	TABLES 10
SUMMARY This study presents the experimental study of some podded propellers with different hub geometry. The experiments were conducted in the cavitation tunnel at Institute for Ocean Technology (IOT), NRC Canada. Four model propellers having the same blade sections but different hub geometry were designed and manufactured and tested at different cavitating conditions. The objective was to investigate the variations of propulsive performance and cavitation characteristics of the propellers because of different hub geometry. Tests were done in various combinations of flow velocity, propeller rotational speed and tunnel pressure. All of the propellers were tested in a wide range of advance coefficients and cavitation numbers to measure propeller thrust and torque. <i>Reynolds Number</i> effects on performance at design cavitation number, effect of hub taper angle on cavitation inception and comparison of performance under various cavitation conditions were investigated. The study gives a suitable basis for comparison of pusher and puller propellers' performance (propeller only case) under cavitating conditions. It is concluded that the puller configuration propellers had better performance than the pusher configuration propellers under majority of test conditions. Results also show that hub taper angle does not have noticeable effect on visual cavitation inception and desinence.			
ADDRESS National Research Council Institute for Ocean Technology Arctic Avenue, P. O. Box 12093 St. John's, NL A1B 3T5 Tel.: (709) 772-5185, Fax: (709) 772-2462			



National Research Council Conseil national de recherches
Canada

Institute for Ocean
Technology

Institut des technologies
océaniques

CAVITATION PERFORMANCE TESTING OF PODDED PROPELLERS WITH DIFFERENT HUB-TAPER ANGLES

TR-2007-04

Mohammed Fakhru Islam and Moqin He

February 2007

Summary

This study presents the experimental study of some podded propellers with different hub geometry. The experiments were conducted in the cavitation tunnel at Institute for Ocean Technology (IOT), NRC Canada. Four model propellers having the same blade sections but different hub geometry were designed and manufactured and tested at different cavitating conditions. The objective was to investigate the variations of propulsive performance and cavitation characteristics of the propellers because of different hub geometry. Tests were done in various combinations of flow velocity, propeller rotational speed and tunnel pressure. All of the propellers were tested in a wide range of advance coefficients and cavitation numbers to measure propeller thrust and torque. *Reynolds Number* effects on performance at design cavitation number, effect of hub taper angle on cavitation inception and comparison of performance under various cavitation conditions were investigated. The study gives a suitable basis for comparison of pusher and puller propellers' performance (propeller only case) under cavitating conditions. It is concluded that the puller configuration propellers had better performance than the pusher configuration propellers under majority of test conditions. Results also show that hub taper angle does not have noticeable effect on visual cavitation inception and desinence.

TABLE OF CONTENTS

Summary	iii
List of Figures	v
List of Tables	vii
Chapter 1. Introduction	1
Chapter 2. Propeller Design and Model Propellers	6
2-1. Propeller Blade Section Geometry	7
2-2. Physical Characteristics of the Propellers	9
Chapter 3. Experimental Set up and Test Conditions	10
3-1. Test Programme	11
3-2. Test Matrix:	12
Chapter 4. Test Procedure And Data Analysis	15
4-1. Podded Propellers Performance under Cavitation	17
4-2. <i>Reynolds Number</i> Effects:	24
4-3. Hub Taper Angle Effects on Performance under Cavitation	28
4-4. Comparison of Push and Pull Configurations under Cavitation	31
4-5. Cavitation and Pattern Observations	38
4-6. Effect of Taper Angle on Cavitation Inception:	40
Chapter 5. Concluding Remarks	42
References	45
Appendix A	47
Appendix B	55

LIST OF FIGURES

Figure 1-1. Propulsion arrangement: Pusher and Puller Podded Propulsors and a conventional Propeller-Rudder System	2
Figure 1-2 (a). Prediction of the pressure distribution at blade root section of the Push+15° propeller	3
Figure 2-1. Podded Propulsion System: puller and pusher systems; definition of hub taper angle	6
Figure 2-2. Four model propellers (physical model). Figure (a), (b), (c), (d) are the propellers with hub taper angles of +15° (push), +20° (pull), -15° (pull), -20° (pull), respectively.	7
Figure 3-1. NRC/IOT Cavitation Tunnel Facility.....	10
Figure 3-2. Pictures of nose and rear cone adapters for the propellers.....	11
Figure 3-3. Solid model for the propellers and nose cone adapters for Push+15 (1 st row) and Push+20 (2 nd row)	12
Figure 4-1. Thrust and torque coefficients and efficiency at atmospheric condition: Propeller-Push+15°	17
Figure 4-2. Thrust and torque coefficients and efficiency at atmospheric condition: Propeller-Push+20°	18
Figure 4-3. Thrust and torque coefficients and efficiency at atmospheric condition: Propeller-Pull-15°	18
Figure 4-4. Thrust and torque coefficients and efficiency at atmospheric condition: Propeller-Pull-20°	19
Figure 4-5. K_T of the propeller, Push+15° at different σ_n . $T_W=19.5^\circ (\pm 0.5^\circ)$; $\alpha/\alpha_s=0.2\sim 0.35$..	20
Figure 4-6. K_Q of the propeller, Push+15° at different σ_n . $T_W=19.5^\circ (\pm 0.5^\circ)$; $\alpha/\alpha_s=0.2\sim 0.35$..	20
Figure 4-7. K_T of the propeller, Push+20° at different σ_n . $T_W=19.5^\circ (\pm 0.5^\circ)$; $\alpha/\alpha_s=0.2\sim 0.35$..	21
Figure 4-8. K_Q of the propeller, Push+20° at different σ_n . $T_W=19.5^\circ (\pm 0.5^\circ)$; $\alpha/\alpha_s=0.2\sim 0.35$..	21
Figure 4-9. K_T of the propeller, Pull-15° at different σ_n . $T_W=19.5^\circ (\pm 0.5^\circ)$; $\alpha/\alpha_s=0.2\sim 0.35$...	22
Figure 4-10. K_Q of the propeller, Pull-15° at different σ_n . $T_W=19.5^\circ (\pm 0.5^\circ)$; $\alpha/\alpha_s=0.2\sim 0.35$..	22
Figure 4-11. K_T of the propeller, Pull-20° at different σ_n . $T_W=19.5^\circ (\pm 0.5^\circ)$; $\alpha/\alpha_s=0.2\sim 0.35$..	23
Figure 4-12. K_Q of the propeller, Pull-20° at different σ_n . $T_W=19.5^\circ (\pm 0.5^\circ)$; $\alpha/\alpha_s=0.2\sim 0.35$..	23

LIST OF FIGURES

Figure 4-13. Performance of the propeller, Push+15° at $\sigma_{design}=3.0$, at three different <i>Reynolds Numbers</i> (three different rps, 15, 20, 25). $T_W=19.5^\circ (\pm 1)$; $\alpha/\alpha_s=0.2\sim 0.35$	26
Figure 4-14. Performance of the propeller, Push+20° at $\sigma_{design}=3.0$, at three different <i>Reynolds Numbers</i> (three different rps, 15, 20, 25). $T_W=19.5^\circ (\pm 1)$; $\alpha/\alpha_s=0.2\sim 0.35$	26
Figure 4-15. Performance of the propeller, Pull-15° at $\sigma_{design}=3.0$, at three different <i>Reynolds Numbers</i> (three different rps, 15, 20, 25). $T_W=19.5^\circ (\pm 1)$; $\alpha/\alpha_s=0.2\sim 0.35$	27
Figure 4-16. Performance of the propeller, Pull-20° at $\sigma_{design}=3.0$, at three different <i>Reynolds Numbers</i> (three different rps, 15, 20, 25). $T_W=19.5^\circ (\pm 1)$; $\alpha/\alpha_s=0.2\sim 0.35$	27
Figure 4-17 (x). Comparison of K_T and K_Q of the Push+15° and the push+20° propellers at σ =variable	29-31
Figure 4-18 (x). Comparison of K_T and K_Q of the Pull-15° and the pull-20° propellers at σ =variable	29-31
Figure 4-19 (x). Comparison of K_T and K_Q of the Push+15° and the pull-15° propellers at σ =variable	32-35
Figure 4-20 (h). Comparison of K_T and K_Q of the Pull-20° and the push+20° propellers at σ =variable	32-35
Figure 4-21. Comparison of thrust coefficient (Push+15° and Pull-15° propellers) variation with cavitation number for fixed advance coefficients	36
Figure 4-22. Comparison of torque coefficients (Push+15° and Pull-15°) at different cavitation numbers for fixed advance coefficients	36
Figure 4-23. Comparison of thrust coefficient (Push+20° and Pull-20° propellers) variation with cavitation number for fixed advance coefficients	37
Figure 4-24. Comparison of torque coefficients (Push+20° and Pull-20°) at different cavitation numbers for fixed advance coefficients	37
Figure 4-25 (x): Comparison of cavitation inception and desinence curves at different J_s for the Push +15°/20° and the Pull-15°/20°) operating at 20/15 rps	41
Figure A-1. Photographs showing back cavitation for 15° Pusher Propeller at different cavitating conditions	47
Figure A-2. Photographs showing back cavitation for -15° Puller Propeller at different cavitating conditions	49
Figure A-3. Photographs showing back cavitation for 20° Pusher Propeller at different cavitating conditions	51

Figure A-4. Photographs showing back cavitation for -20° Puller Propeller at different cavitating conditions 53

LIST OF TABLES

Table 2-1: Basic geometry of the model propeller 7

Table 2-3. Sectional geometry offsets for the model propeller in the radial direction (values normalized by propeller diameter)..... 8

Table 2-4. Model propeller sectional maximum thickness and camber distribution. Here, x/c is the normalized distance from leading edge; t/c is sectional thickness and f/c is sectional camber. All values are normalized by local chordlength,..... 8

Table 2-5. Physical characteristics of the model propellers 9

Table 3-1. Summary of test conditions 13

Table 3-2. Calculation of tunnel absolute pressure for different cavitation numbers tested 14

Table 4-1. Test parameters in the current experimental stud..... 16

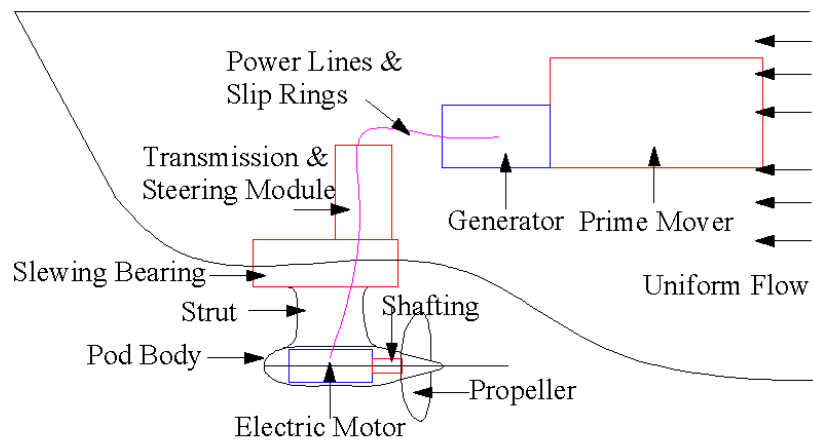
Table 4-2. Non-dimensional performance coefficients used to present the experimental results. 16

Table 4-3. Calculation of *Reynolds Number* for three different propeller rps. 24

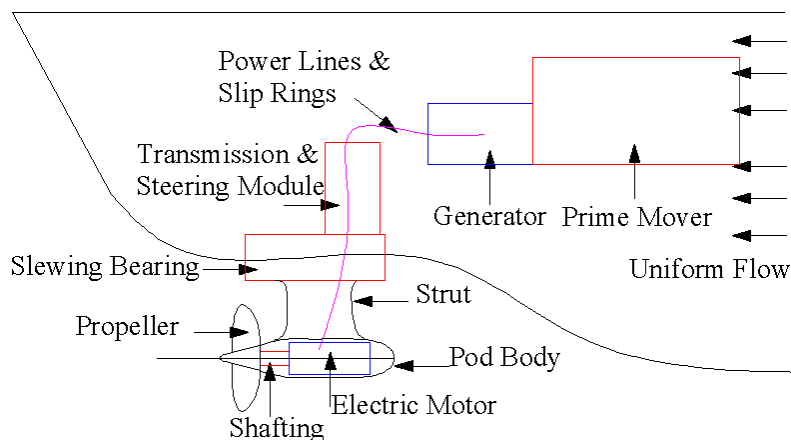
Table B-1. Experimental data of the four propellers at different cavitating conditions 55

Chapter 1. Introduction

The podded propulsor units are integrated propulsion and steering systems that eliminate the need for the rudder, long shafts and gears of traditional propulsion systems. The propeller is driven by an electric motor that resides in a torpedo like body called pod or gondola or nacelle. The strut that connects the pod to the hull acts in place of the rudder and the propeller turns and creates a thrust at an angle, which is an added steering force. Figure 1-1 depicts the two configurations of currently used podded propulsors together with a conventional propulsion system. Basically, two configurations are mostly used in commercial field: puller configuration and pusher configuration. In the puller system (see Figure 1-1a), a propeller is fitted forward of the pod and operated in the wake of ship (almost uniform inflow condition) whereas, in the pusher system (see Figure 1-1b), the propeller is fitted aft of the pod and operated in the wake of ship and the strut.



Podded Propulsor in Puller Configuration



Podded Propulsor in Pusher Configuration

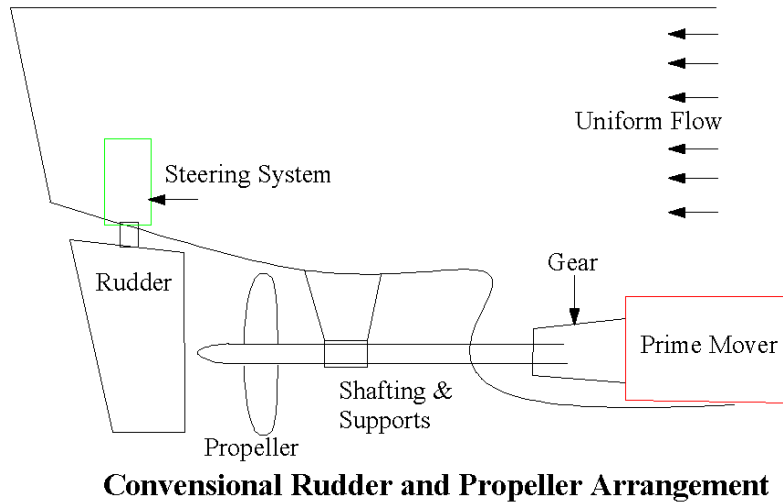


Figure 1-1. Propulsion arrangement: Pusher and Puller Podded Propulsors and a conventional Propeller-Rudder System.

Currently, the majority of the commercial vessels are equipped with puller podded propulsion systems. It is known from the shipbuilders that the pusher propellers yield a lower thrust and hence less propulsive efficiency as compared to the puller ones. A study was performed to investigate why this is so (Islam *et al.* 2004). In the study we found that the pressure distribution around the blade root sections are very poor due to the abnormal blade sectional shape created by the intersection of the blade body and the hub (positive hub taper angle means reduced diameter downstream). Pusher and puller podded propellers have opposite hub taper angle, hence different blade root sections. In that study by Islam (2004), it was found that hub taper angle has considerable effects on the open water performance of podded propellers. The reason for the poor performance of a pusher propeller was attributed to the sectional pressure distributions at the blade root sections (see Figure 1-2). As shown in Figure 1-2(a), the pressure difference between the suction side and the pressure side, after mid-chord, produced negative thrust for the pusher propeller. Figure 1-2(b) shows the pressure coefficient distribution over the suction side and the pressure side and the distribution is more normal leading to better thrust for the puller propeller. This variation of performance of the two propellers may or may not be similar for operation under cavitation. Further investigations are required to examine the variation, if any, of the performance of the pusher and puller propellers at different cavitating conditions.

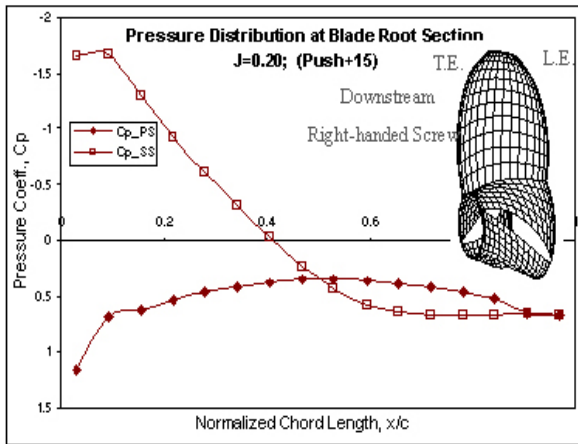


Figure 1-2 (a). Prediction of the pressure distribution at blade root section of the Push+15° propeller.

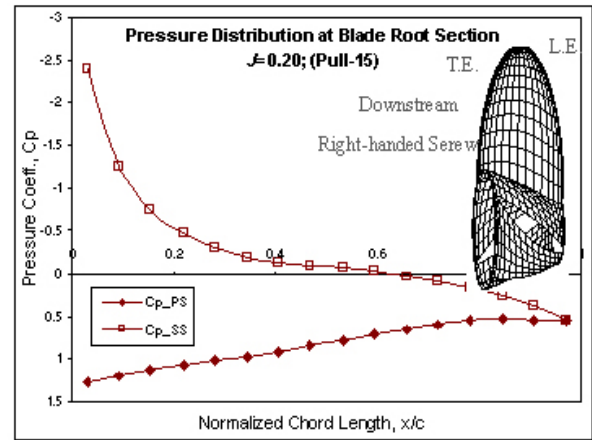


Figure 1-2 (b). Prediction of the pressure distribution at blade root section of the Pull-15° propeller.

The occurrence of cavitation on marine propellers causes undesirable effects such as radiated noise, structural vibration, blade surface erosion and deterioration of performance. The propellers used in a podded propulsion system are vulnerable to various kind of cavitation due to the change of surrounding flow field as compared to a conventional propeller-rudder propulsion system. The flow condition of a pusher and a puller propeller are different, which induces different cavitation characteristics.

There have been studies into the performance, cavitation and accompanying noise characteristics of propellers with various propeller geometries. Gawn and Burrell (1957) presented valuable and extensive results in terms of performance of thirty propellers made to the same design, but having combination of different blade area ratios and face pitch ratios at several cavitation numbers over a wide range of slip. Denny (1968) presented the results of cavitation inception and performance tests for a series of model propellers designed using lifting surface procedure(s). Matsuba *et al.* (1994) presented extensive experimental results on the hydrodynamic characteristics of nine supercavitating propellers performed at the SRI large cavitation tunnel using new and improved measurement procedures.

Walker (1995) studied the cavitation properties of propeller blade root fillet geometries through model tests. Walker (1996) performed a comprehensive study on the effects of blockage and cavitation on the hydrodynamic loads associated with non-contact propeller ice interaction. The tests were conducted in uniform flow and in blocked flow using simulated ice blockages installed upstream of the propeller. Pustoshny and Kaprantsev (2001) reported some results of observations of full-scale propeller blade cavitation patterns for different manoeuvring modes. Atlar *et al.* (2001) presented the results of cavitation tunnel tests of a

model propeller of a research vessel and those of noise measurements with its full-scale propeller. Pereira *et al.* (2002) gave the results of new experimental developments into the observation and quantification of the cavitation pattern for a skewed four-blade model propeller in a uniform inflow. In a recent investigation Pereira *et al.* (2004) measured the pressure and noise around a cavitating propeller in non-uniform flow field using high-speed visualization techniques.

Friesch (2001 and 2004) used ship models in cavitation tunnel to study various aspects of podded propulsor. He measured the cavitation behavior combined with pressure fluctuation and noise for different pod arrangements. He measured propeller thrust, torque and revolution at the shaft and unit thrust and side forces of the propulsors using a force balance placed in the ship model. The pod units were fitted to an adjustable frame to test the model at different azimuthing and tilt angles. Large rotational speeds (up to 35 rps) and model propeller diameters (210~260 mm) were used to reach high *Reynolds Number* comparable with those for conventional propeller shaft arrangements. Based on the analyses the author stated that there is an advantage for podded propulsors in puller configurations in terms of vibration and noise behavior. It is also recommended, for high-speed vessels, pod propellers with higher number of blades of lower diameter to achieve improved cavitation behavior with small loss of efficiency.

Szantyr (2001a) presented results of a series experiments, which were conducted in a cavitation tunnel and observation was made of a symmetric pod unit in the pushing, pulling and combined (tandem propeller; each fitted at one end of the pod) modes for different azimuthing angles. The emphasis was placed on the interaction between the pod body and the cavitation tip vortex system of the propeller(s). It was concluded that the presence of the strut noticeably distorted the free vortex system, especially in the puller and combined systems. The effect of the pod on the geometry of the free vortex system of the fore propeller was reported rather small.

Heinke (2004) reported on a set of systematic model tests, some of which were carried out in a large circulating and cavitation tunnel, with a 4- and 5-blade propeller in pull and push mode fitted to a generic pod housing. In order to study the cavitation behavior the author measured the forces and moments on the propeller and the pod body at different steering angles at conditions for zero rps, low number of revolutions (simulating crash stop) and at the design speed and revolutions with dynamically turning pod. The latter case, which may represent an unrealistic operating condition at large steering angles, presents a strong flow separation and cavitation leading to a reduction of propeller torque and thrust.

To the authors' knowledge, the present work would be the first attempt to study the effects of hub taper angle on performance of a propeller designed for podded propulsion systems under cavitating conditions. It is very important to perform a comparative study of a puller and a pusher podded propeller at several cavitation conditions. This will help in judging the relative performance deterioration of these two propellers under cavitation and the superiority of one over the other. The current experimental study was carried out to fill this knowledge gap in understanding the hydrodynamics of podded propulsors under cavitation. The cavitation tunnel tests, which were carried out at the cavitation tunnel at the Institute for Ocean technology (IOT), National Research Council (NRC) Canada, involved measurements of the performance of four propellers with different hub taper angles under several cavitating conditions. Observation of the cavitation characteristics and visual cavitation inception tests were also performed. The cavitation inception tests were conducted with a view to examine the effects of hub taper angle on cavitation inception. Additional tests were done at the design cavitation number with three different propeller rotational speeds to investigate the *Reynolds Number* effects at design conditions. The experiments occupied much of the operating time of the tunnel over a period of four weeks exclusive of calibration and set-up time. More than 800 individual propeller test runs were done and about 18 hours of video footage of cavitation pattern was recorded. A complete account of the investigation is given in the following sections. The results are presented in a format suitable for the use of propeller designers. The details of the model propellers are given in chapter 2. Chapter 3 details the experimental set-up and test conditions. In chapter 4, all the experimental results and relevant discussions for the performance of the propellers are provided in several formats. Finally, in chapter 5 some concluding remarks and suggestions for future research are provided. All the pictures representing the propellers operating at different cavitating conditions are presented in Appendix A. The experimental data is provided in Appendix B.

The report was written to provide the information provided will form a good basis of validation for numerical work. Also, the data will be useful for design optimization and development for podded propellers over a wide range of conditions, including those, which involve cavitation.

Chapter 2. Propeller Design and Model Propellers

The four model propellers have the same blade sections with different hub taper angles. Figure 2-1 shows the definition of hub taper angle and the difference between the two major types of podded propulsion systems as described in the study by Islam *et al.* (2004). The basic geometrical particulars of the propellers are given in Table 2-1 (Liu 2006). The propeller is named as PP00+00C0 and its key points are summarized in Table 2-1. The name is explained as P for podded, P for propeller, 00 for zero skew, +00 for zero positive rake, C/V for constant or a variable pitch and 0/1/2.... for cavitation number to be used. The four propellers have hub taper angles of 15° (right handed pusher configuration, **Push+15°**), 20° (right handed pusher configuration, **Push+20°**), -15° (left handed puller configuration, **Pull-15°**), -20° (right handed puller configuration, **Pull-20°**). Figure 2-2 shows a photograph of the model propellers.

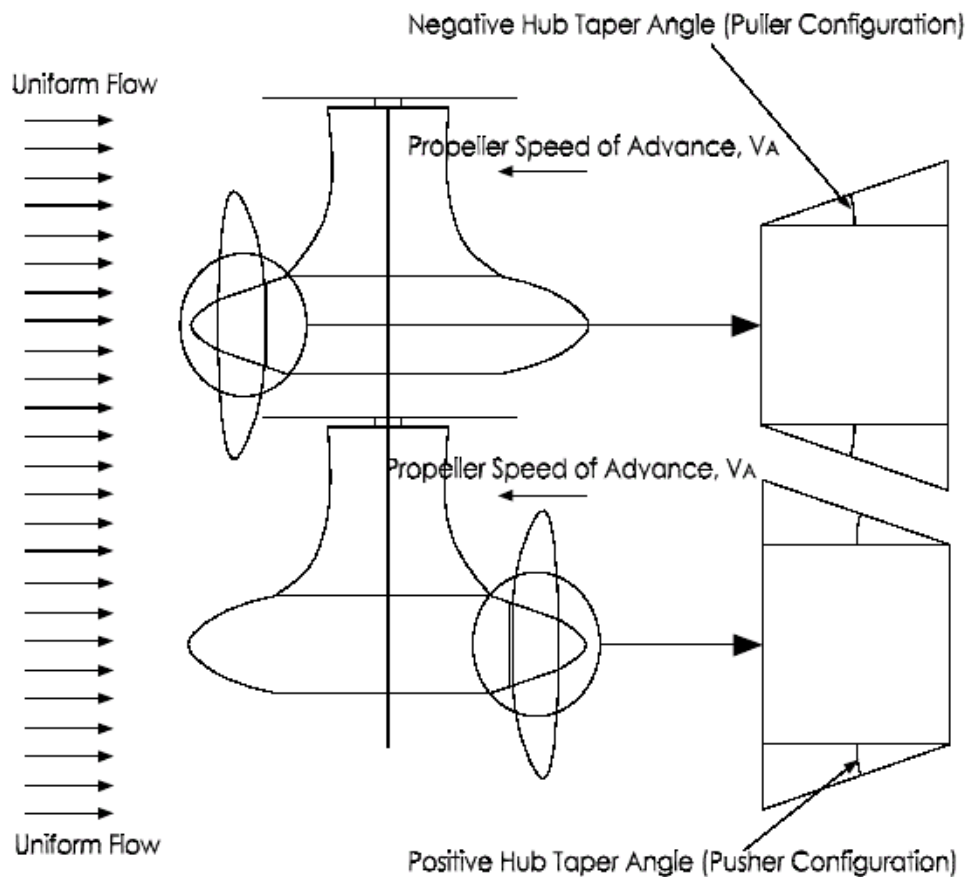


Figure 2-1. Podded Propulsion System: puller and pusher systems; definition of hub taper angle.

Table 2-1: Basic geometry of the model propeller.

Diameter (m)	0.27
No. of Blade	4
Design advance coefficient, J	0.8
Hub-Diameter (H/D) ratio	0.26 (based on regular straight hub)
Angular speed (rps)	25
Section thickness form	NACA 66 (DTMB Modified)
Section meanline	NACA = 0.8
Blade planform shape	Blade planform shape was based on David Taylor Model Basin model P4119 [12]
Expanded area ratio, EAR	0.60
Pitch distribution	Constant, $P/D=1.0$
Skew distribution	Zero
Rake distribution	Zero



Figure 2-2. Four model propellers (physical model). Figure (a), (b), (c), (d) are the propellers with hub taper angles of +15° (push), +20° (pull), -15° (pull), -20° (pull), respectively.

2-1. Propeller Blade Section Geometry

The propeller blade section is a version of the NACA 66 (DTMB modified) foil, using a $A=0.8$ meanline. The sectional geometry offsets are included in the Tables 2-3 and 2-4. In the tables, r is local radius, c is local chord length, p local pitch, α is local skew angle, β is local rake angle, t_{max} local maximum thickness and f_{max} is local maximum camber.

Table 2-3. Sectional geometry offsets for the model propeller in the radial direction (values normalized by propeller diameter).

r	c	p	α	β	t_{max}	f_{max}
0.30	0.285550	1.00	0.00	0.00	0.15530	0.02318
0.40	0.318870	1.00	0.00	0.00	0.11800	0.02303
0.50	0.345968	1.00	0.00	0.00	0.09160	0.02182
0.60	0.363141	1.00	0.00	0.00	0.06960	0.02072
0.70	0.364086	1.00	0.00	0.00	0.05418	0.02003
0.80	0.342423	1.00	0.00	0.00	0.04206	0.01967
0.90	0.284605	1.00	0.00	0.00	0.03321	0.01817
0.95	0.218593	1.00	0.00	0.00	0.03228	0.01631
1.00	0.126036	1.00	0.00	0.00	0.03160	0.01175

Table 2-4. Model propeller sectional maximum thickness and camber distribution. Here, x/c is the normalized distance from leading edge; t/c is sectional thickness and f/c is sectional camber. All values are normalized by local chordlength, c .

x/c	t/c	f/c
0.0000	0.0000	0.0000
0.0125	0.2088	0.0907
0.0250	0.2932	0.1586
0.0500	0.4132	0.2712
0.0750	0.5050	0.3657
0.1000	0.5814	0.4482
0.1500	0.7042	0.5869
0.2000	0.8000	0.6993
0.3000	0.9274	0.8635
0.4000	0.9904	0.9615
0.4500	1.0000	0.9881
0.5000	0.9924	1.0000
0.6000	0.9306	0.9786
0.7000	0.8070	0.8892
0.8000	0.6220	0.7027
0.9000	0.3754	0.3586
0.9500	0.2286	0.1713
1.0000	0.0666	0.0000

The manufacturing of the model propellers was completed at Memorial University St. John's Campus, using CNC vertical machining center. The propeller geometry was input into the panel method code PROPELLA, which in addition to providing numerical simulation of the models, output *.dxf files for the propeller geometry. The files were then modified and used by the CNC machining center to manufacture the propeller. The manufacturing tolerance for the CNC machining is $\pm 0.0001\text{m}$ (Kavanagh 2004).

2-2 Physical Characteristics of the Propellers

The physical characteristics of the model propellers are given in Table 2-5.

Table 2-5. Physical characteristics of the model propellers.

Propeller Name	Push+20°	Propeller Name	Push+15°
Scale, λ	18.5 to 1	Scale, λ	18.5 to 1
Number of Blades, Z	4	Number of Blades, Z	4
Full Size Diameter, D	5.0 m	Full Size Diameter, D	5.0 m
Average Model Diameter, Dm	0.27 m	Average Model Diameter, Dm	0.27 m
Blade Area Ratio, AE/A0	0.60	Blade Area Ratio, AE/A0	0.60
Pitch ration at 0.7R, P/D	1.0	Pitch ration at 0.7R, P/D	1.0
Material	Bronze	Material	Bronze
Model Mass	2579.39 gm.	Model Mass	2201.91 gm.
Hub Taper Angle	+20°	Hub Taper Angle	+15°

Propeller Name	Pull-20°	Propeller Name	Pull-15°
Scale, λ	18.5 to 1	Scale, λ	18.5 to 1
Number of Blades, Z	4	Number of Blades, Z	4
Full Size Diameter, D	5.0 m	Full Size Diameter, D	5.0 m
Average Model Diameter, Dm	0.27 m	Average Model Diameter, Dm	0.27 m
Blade Area Ratio, AE/A0	0.60	Blade Area Ratio, AE/A0	0.60
Pitch ration at 0.7R, P/D	1.0	Pitch ration at 0.7R, P/D	1.0
Material	Bronze	Material	Bronze
Model Mass	2575.50 gm.	Model Mass	2240.70 gm.
Hub Taper Angle	-20°	Hub Taper Angle	-15°

Chapter 3. Experimental Set up and Test Conditions

The experiments were carried out at the Institute for Ocean technology (IOT) cavitation tunnel facility. Doucet (1992) detailed the tunnel configuration. The tunnel is a closed water circuit with a 2.2 m × 0.5 m × 0.5 m cross-section with rounded corners (radius of 60 mm). Optical access to the section is possible through large plexi-glass windows. The water speeds ranges from 0.0 m/s to 10.0 m/s. The propeller rotational speed ranges from 0 rps to 30 rps. The test section pressure (absolute) ranges from 10 kPa to 200 kPa. Figure 3-1 shows the schematic view of the cavitation tunnel (taken from IOT website).

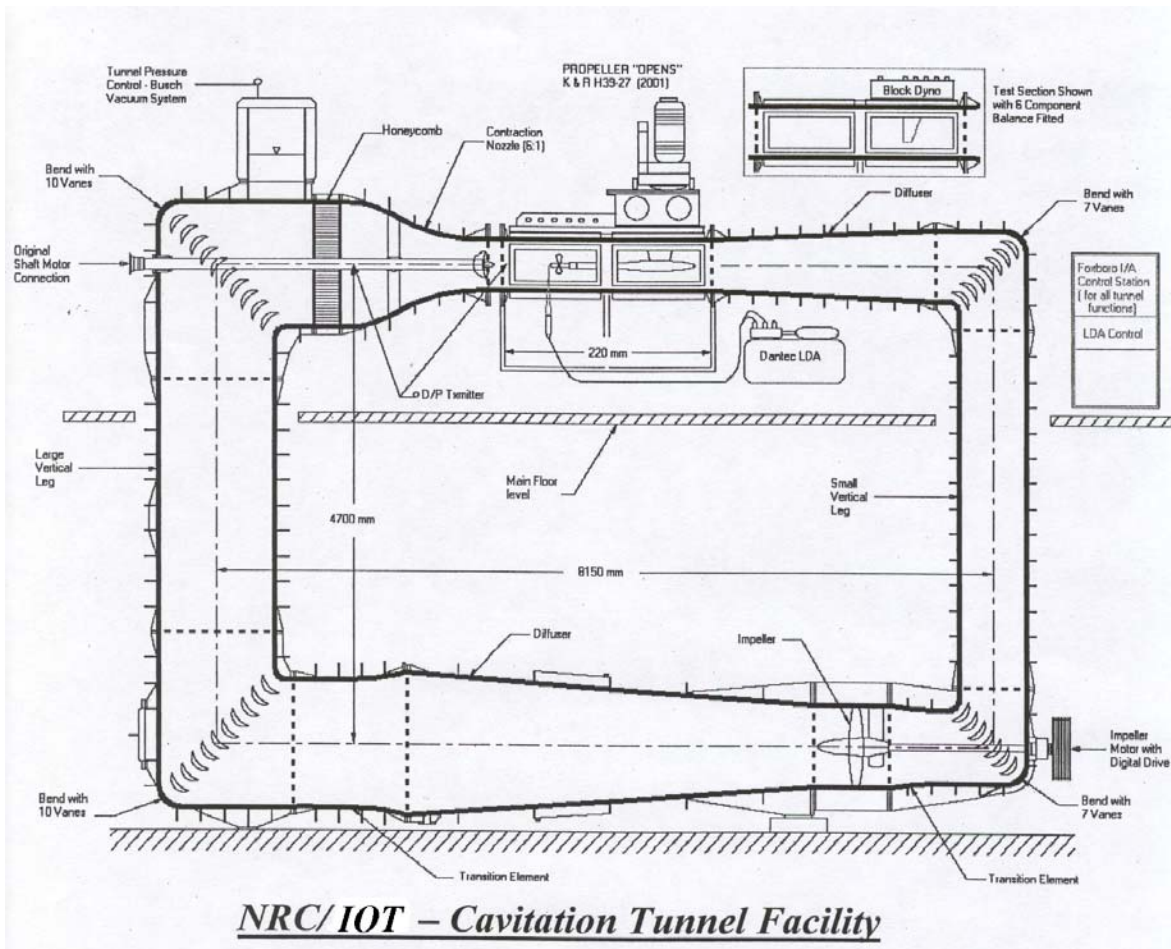


Figure 3-1. NRC/IOT Cavitation Tunnel Facility.

The tunnel is equipped with Foxboro software, which allows for a precise control of propeller rotation, flow, pressure, and filtration conditions. All torque and thrust measurements were made using a sealed strain gauge dynamometer (*Kempf & Remmers*) mounted between the

propeller and first shaft bearing with a ± 900 N thrust range and ± 45 Nm torque range. All pressure and flow measurements were made using pressure transducers, and the rotational speed of the propeller was measured using a digital tachometer. An oxygen sensor was used to give the gas content measurements to ensure proper cavitation scaling (Brent 2004).

Figure 3-1 shows a schematic view of the cavitation tunnel. The detailed procedure for operating the cavitation tunnel, including its water and vacuum system, manometry, model installation and emergency procedure are to be found in Doucet (1992) and the reader is referred to that work for step-by-step instructions.

3-1. Test Programme

All of the four propellers were fitted to the shaft line of the dynamometer in the cavitation tunnel. Some aft fairing, forward cone and adapters were required to ensure smooth flow into the propeller. Figure 3-1 shows all the accessories required for the tests.



Figure 3-2. Pictures of nose and rear cone adapters for the propellers.

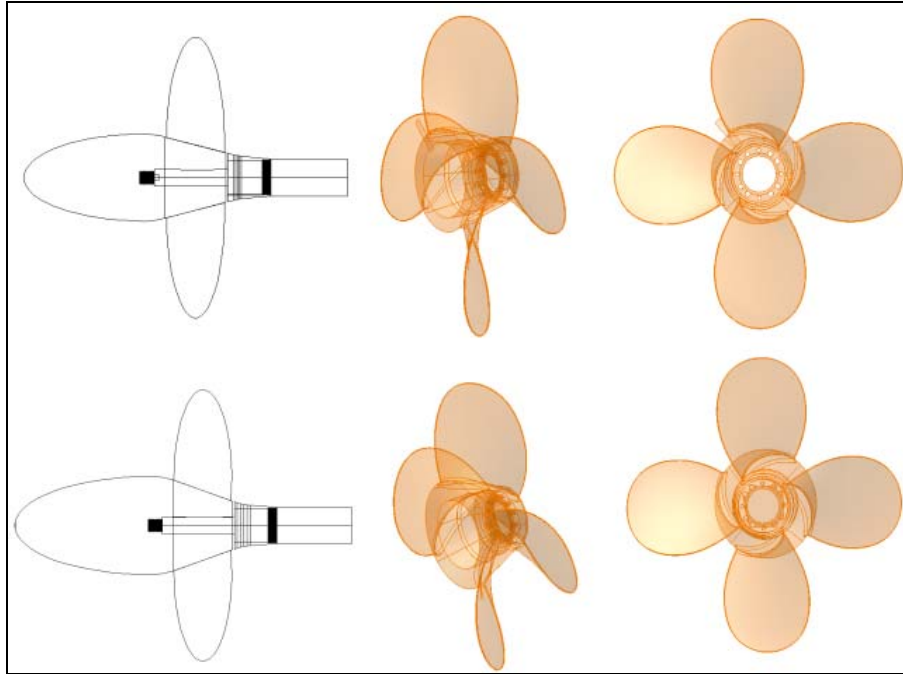


Figure 3-3. Solid model for the propellers and nose cone adapters for Push+15 (1st row) and Push+20 (2nd row).

3-2. Test Matrix:

The test matrix was comprised of basically four different types of tests:

- ✓ For each of the four propellers, at constant propeller rotational speed of 25 rps, the tunnel pressure was varied from atmospheric pressure to the lowest attainable without tunnel vibrations. At each tunnel pressure the flow velocity was varied to measure propeller thrust and torque at different advance coefficients, J .
- ✓ For each propeller at design cavitation number, the propeller forces were measured at three different propeller rps of 15, 20 and 25 with the similar range of advance coefficients. These tests were done to observe any *Reynolds Number* effect.
- ✓ For each conditions mentioned above, a visual cavitation inception and desinence were recorded using digital videotapes and pictures.

The basic test matrix outline is given in Table 3-1. Four model propellers were tested at nine cavitation numbers including the cavitation number at the atmospheric pressure. For each set up, the propeller rotational speed and the static pressure in the measuring sections were maintained constant while thrust, torque and the water speed were measured over a range of advance coefficients, J .

Table 3-1. Summary of test conditions.

Test Item.	Rotational Speed, rps	Constant Tunnel Pressure, P_t (psi)	Flow Velocity V_A (m/s)
1	25	1.23	3.8-7.5
2	25	1.90	3.8-7.5
3	25	2.56	3.8-7.5
4	25	3.22	3.8-7.5
5	25	4.54	3.8-7.5
6	25	5.86	3.8-7.5
7	25	9.16	3.8-7.5
8	25	14.12	3.8-7.5
9	25	14.69	3.8-7.5
10	20	9.16	3.2-7.25
11	15	9.16	2.6-6.75

In establishing the test conditions in table 3-1, the following formula (Liu, Bose and Colbourne 2002) was used for reference (or nominal) cavitation number, σ_n for a propeller at the shaft centre:

$$\sigma_n = \frac{P_{amb} + \rho gh - P_V}{\frac{1}{2} \rho n^2 D^2} \quad (3.1)$$

where, P_{amb} is the ambient pressure on the fluid surface in Pa or N/m², ρ is the density of the fluid in kg/m³, g is gravitational acceleration, taken as 9.8 m/s² and h is the immersion depth of the propeller centre (the intersection of the shaft centre line and the directrix of the propeller, which is also normally the origin of the propeller geometry) in m. This definition is also valid for propellers with an inclined shaft in oblique flow. P_V is the saturated vapor pressure in Pa, which is a function of temperature and type of fluid. Variable n is the angular speed of the propeller in rad/s and D is the diameter of the propeller in metres. In practical ship navigation, the value of the ambient pressure P_{amb} is equal to the atmospheric pressure, which is usually represented by P_{atm} .

The ambient pressure on the surface of the fluid is a function of the cavitation number in both physical and numerical modeling processes. For example, to obtain a given cavitation number during a test in a cavitation tunnel, the local ambient pressure of the facility must be varied. For a given temperature, fluid, propeller angular speed and diameter, the cavitation number controls the ambient pressure of fluid surface, P_{amb} , through equation 3.2 (Liu, Bose and Colbourne 2002):

$$P_{amb} = \frac{1}{2} \rho n^2 D^2 \sigma_n - \rho gh + P_V \quad (3.2)$$

In the equations 3-1 and 3-2, the nominal cavitation numbers are based on propeller revolutions instead of propeller advance speed or propeller resultant speed. These

formulations give the advantage of presenting the performance in terms of thrust coefficient, K_T or torque coefficient, K_Q against cavitation number, which is not a function of advance coefficient, J .

Table 3-2 presents the nominal cavitation numbers that were tested along with the corresponding absolute tunnel pressure to achieve the cavitation number under the specified operating conditions. In the calculation, the vapor pressure at an average water temperature of 19° was used, although the water temperature varied $\pm 1^\circ$ during the experiments.

Table 3-2. Calculation of tunnel absolute pressure for different cavitation numbers tested.

σ_n	ρ (Kg/m ³)	n (rev/s)	D (m)	P_v (N/m ²)	g (m/s ²)	h (m)	P_{tun_abs} (N/m ²)	P_{tun_rel} (N/m ²)	P_{atm} (N/m ²)	P_{tun_abs} (psi)
0.6	1000	25	0.27	2300	9.81	0.76	8513.15	-92786.85	101300	1.23
0.8	1000	25	0.27	2300	9.81	0.76	13069.40	-88230.60	101300	1.90
1	1000	25	0.27	2300	9.81	0.76	17625.65	-83674.35	101300	2.56
1.2	1000	25	0.27	2300	9.81	0.76	22181.90	-79118.10	101300	3.22
1.6	1000	25	0.27	2300	9.81	0.76	31294.40	-70005.60	101300	4.54
2	1000	25	0.27	2300	9.81	0.76	40406.90	-60893.10	101300	5.86
3	1000	25	0.27	2300	9.81	0.76	63188.15	-38112.85	101301	9.16
4.5	1000	25	0.27	2300	9.81	0.76	97360.03	-3941.98	101302	14.12
7.38 (σ_{atm})	1000	25	0.27	2300	9.81	0.76	101300.00	0.00	101300	14.69

A rotational speed of 25 rps was used in order to get low cavitation numbers below 1.0 using the current facility (see equation 3-1). The propellers were also tested at two additional shaft speed of 15 rps and 20 rps at the design cavitation number of $\sigma_{design} = 3.0$ (≈ 2.9894) in order to study the *Reynolds Number* effects on the propeller performance. Video footage for all experimental conditions was taken. Later, photographs were extracted from the video clips at different operating conditions at all cavitation numbers. The air content number, α/α_s (Matsuba *et al.*, 1994) during the experiments varied from 0.2 to 0.4. The tunnel was de-aerated several times to keep the air content level under satisfactory conditions.

The propellers were mounted on the upstream shaft with an axially uniform inflow. While doing the tests, the tunnel static pressure and propeller rotation speed were fixed based on the required cavitation number. After the tunnel flow was stabilized, the flow speed was changed gradually to get the required advance coefficients, keeping the rotational speed fixed. Propeller thrust and torque were measured at each operating condition. Observation of the cavitation patterns was made and different cavitation characteristics were noted with sketches for all the experimental conditions.

Chapter 4. Test Procedure and Data Analysis

All of the four propellers were tested at different tunnel pressures. The propeller rotational speed, n was held constant and the speed of advance of the propeller, V_A was varied from the lowest attainable to a limit where excessive tunnel vibration could be avoided. During the experiments, thrust, torque, speed of advance, rotational speed and tunnel pressure were measured. In addition, the water temperature and air content (% oxygen dissolved in the water) were recorded before, during and after each experiment to maintain standard cavitation test conditions (ITTC recommended procedure: 7.5-02-03-03.1). The combination of propeller size (270 mm) and rotational speed (25 rps) were selected to ensure high *Reynolds Number* (over 1 million) to avoid any adverse effect of laminar flow over the propellers (dynamic stall of the propeller blades, details given in section 4-2). The calibration of the dynamometer was done following standard ITTC recommended procedure: 7.6-02-08 and 09. The measurements included:

- Propeller shaft thrust and torque
- Shaft rotational speed
- Facility flow reference velocity
- Static pressure
- Temperature
- Air Content, Water quality measure

The measured torque was corrected for bearing torque in order to determine the propeller torque. This shaft or friction loss was determined by running friction tests before and after the tests in each day till the end of the whole test program. In a friction test, two cylindrical dummy hubs were fitted to the shaft in place of the propellers. The dummy hubs have the almost the same mass (2% difference) as the actual propellers, but does not develop a thrust on the shaft. Friction torque load is measured as the shaft speed is varied throughout its operating range (at zero water speed). A tunnel boundary correction was also made to account for the effect of the tunnel walls on the water flow (Lindgren 1963). Besides the velocity corrections, corrections on the cavitation number were applied in the data analysis (Lindgren 1963). The test parameters are summarized in Table 4-1.

Table 4-1. Test parameters in the current experimental study.

Parameter	Recommended Values	Test Values
Pressure adjustment to	0.7 ~ 0.9 R	0.7R
Blockage	Less than 20 % of test section size	0.23 (blockage correction is necessary)
Number of revolutions of model propeller	As high as possible in accordance with tunnel speed	25, 20 and 15
Minimum Reynolds-numb	Minimum value of 0.5 million based on the blade chord length at 0.7 R	Min attained was over 1 million.
Number of pressure transducers	5 ~ 20	N/A
Air content / nuclei Distribution	As high as possible according to the facility experience. Values of total air content or Oxygen content should be mentioned	Around 20%
Noise	Low values of the facilities	Reasonably low
Reproducibility	At least two different rotation rates of the model propeller should be tested	Three different rotation rates
Model propeller diameter	> 200 mm	270 mm

The results of the tests are presented in the form of plots of non-dimensional performance coefficients as shown in Table 4-2. Thrust and torque coefficients, K_T and K_Q respectively, and propulsive efficiency, η were presented against advance coefficients, J .

Table 4-2. Non-dimensional performance coefficients used to present the experimental results.

Basic Measured Data		Derived Data	
Representative static pressure at propeller radius 0.8	p	Cavitation number	$\sigma_n = \frac{P_{amb} + \rho gh - P_V}{\frac{1}{2} \rho n^2 D^2}$
Rotational velocity rps	n	Thrust Coefficient, K_T	$K_T = T / (\rho n^2 D^4)$
Tunnel speed m/s	V_{Tunnel}	Torque Coefficient, K_Q	$K_Q = Q / (\rho n^2 D^5)$
Propeller thrust N	T	Advance Coefficient, J	$J = V_A / (nD)$
Propeller torque Nm	Q	Propeller Efficiency, η	$\eta = (J / (2\pi)) \times (K_T / K_Q)$
Water temperature °C	t	Vapor Pressure	P_V
Air Content /	v / v_s		

Oxygen Content			
-------------------	--	--	--

4-1. Podded Propellers Performance under Cavitation

The basic results of the experiments are given as curves of thrust coefficient, K_T , torque coefficient, K_Q , and efficiency, η , to a base of advance coefficient, J , for each cavitation number, σ_n . The atmospheric pressure test results for the four propellers are shown in Figures 4-1 to 4-4. It is observed that the puller configuration propeller with 15° hub angle had higher propulsive efficiency than the pusher propeller with 15° hub angle; whereas the pusher propeller with 20° hub angle had higher propulsive efficiency than puller configuration propeller with 20° hub angle at all advance coefficients. A more elaborate comparative study is presented in the following sections of the report. A detail study on the uncertainty of the measuring equipment is provided in Taylor (2006).

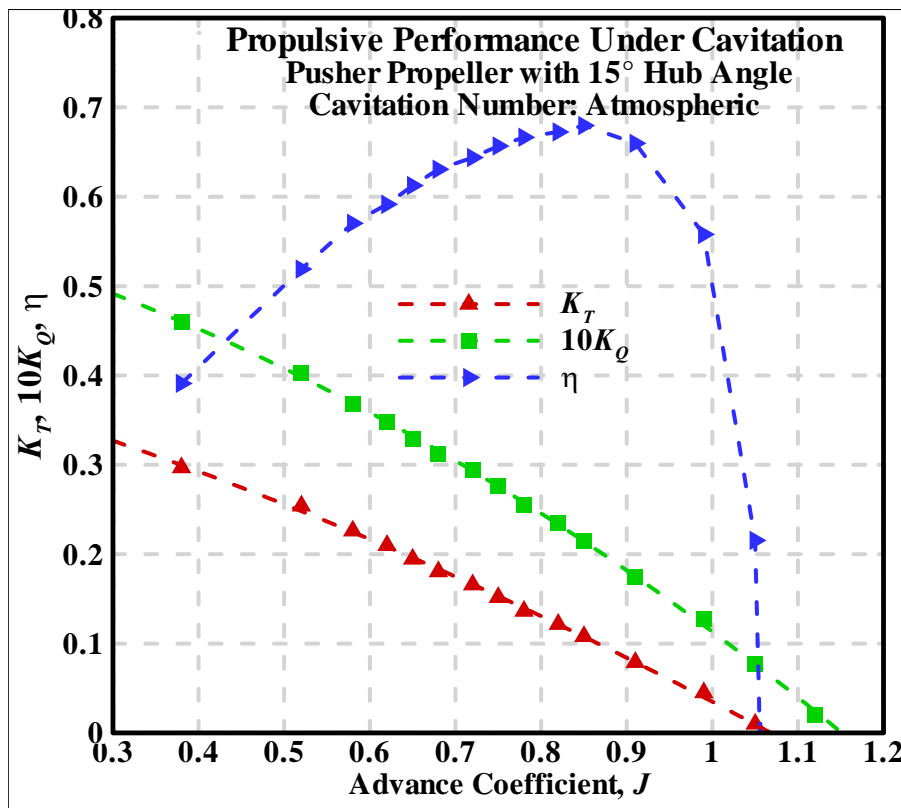


Figure 4-1. Thrust and torque coefficients and efficiency at atmospheric condition: Propeller-Push+ 15° .

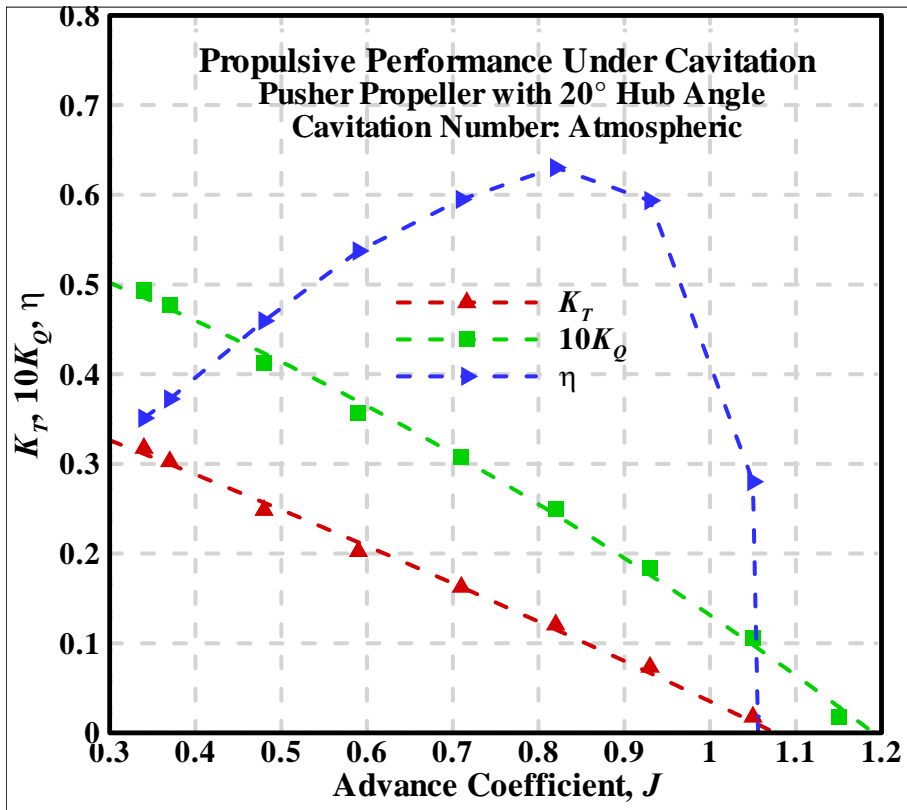


Figure 4-2. Thrust and torque coefficients and efficiency at atmospheric condition: Propeller-Push+20°.

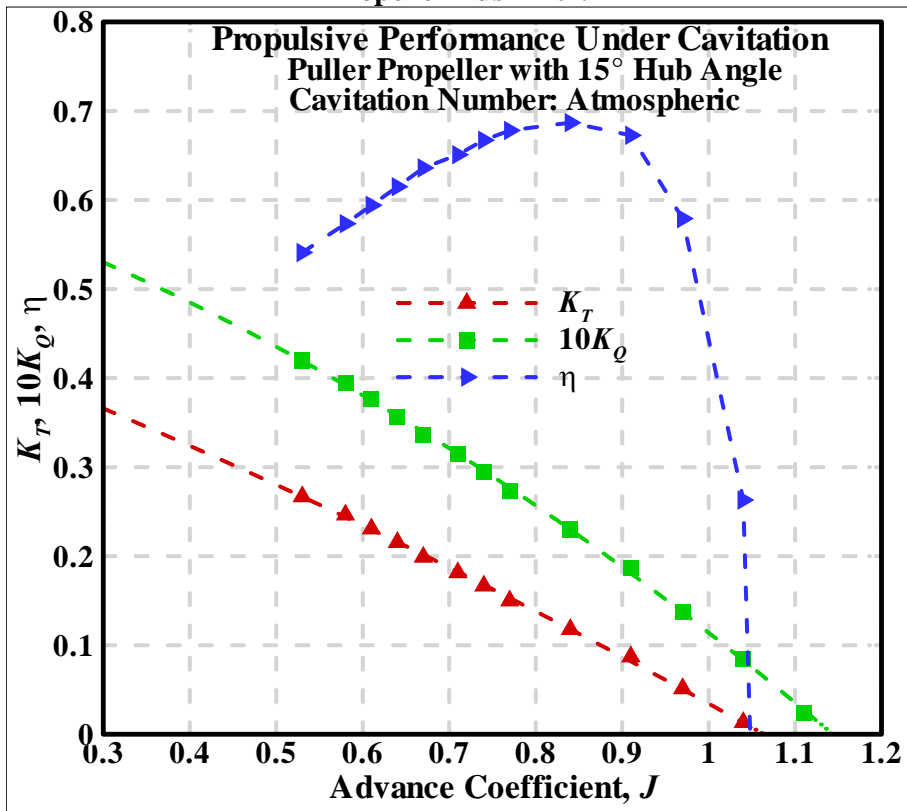


Figure 4-3. Thrust and torque coefficients and efficiency at atmospheric condition: Propeller- Pull-15°.

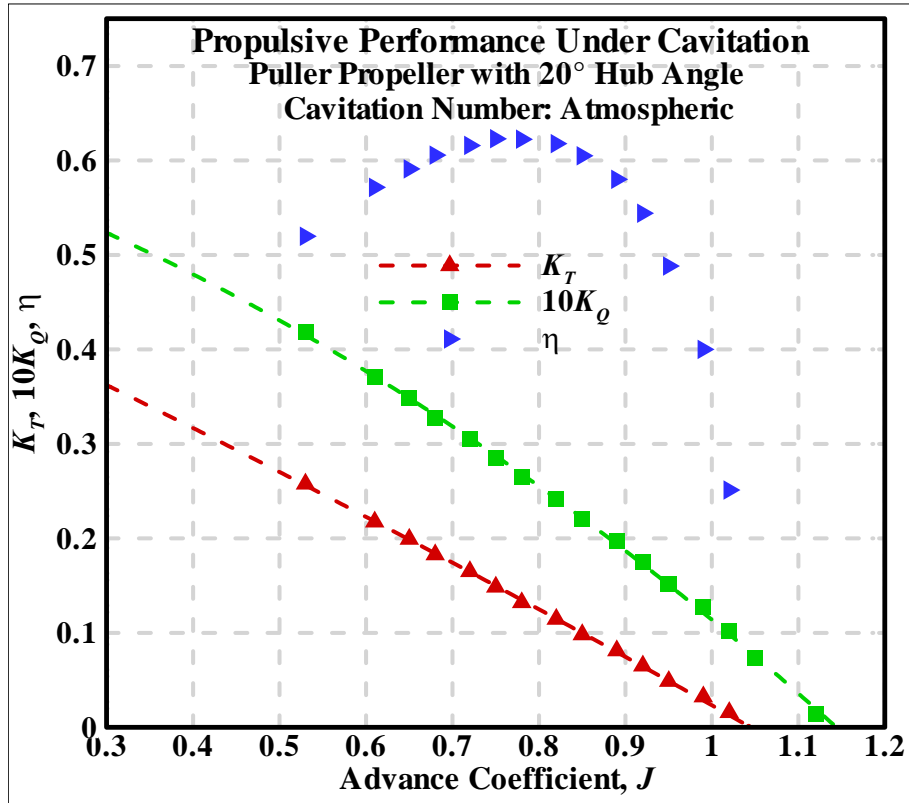


Figure 4-4. Thrust and torque coefficients and efficiency at atmospheric condition: Propeller- Pull-20°.

Figure 4-5 to 4-12 show the thrust and torque coefficients of the four propellers under several cavitating conditions. Here, for different cavitation numbers the lowest achievable advance coefficients varied because of the high rotational speed of the propellers. The propellers running at high rotational speed induced flow into the propeller so that even though the flow speed was nominally zero, the actual inflow was non-zero. The data of the all the tests is provided in tabular form in Table B-1 in Appendix B.

It can be seen from Figures 4-5 to 4-12 that the cavitation effects on K_T as well as on K_Q were limited to the range of cavitation number $\alpha_n < 1.6$ for all four-propeller configurations. As the cavitation number decreases, the produced thrust and torque decreases. As the cavitation number decreases the amount of cavitation (mainly sheet cavitation) on the blade surface area on the suction side of the propeller blades increases, which deteriorates both K_T and K_Q (see Figures A-1 to A-4).

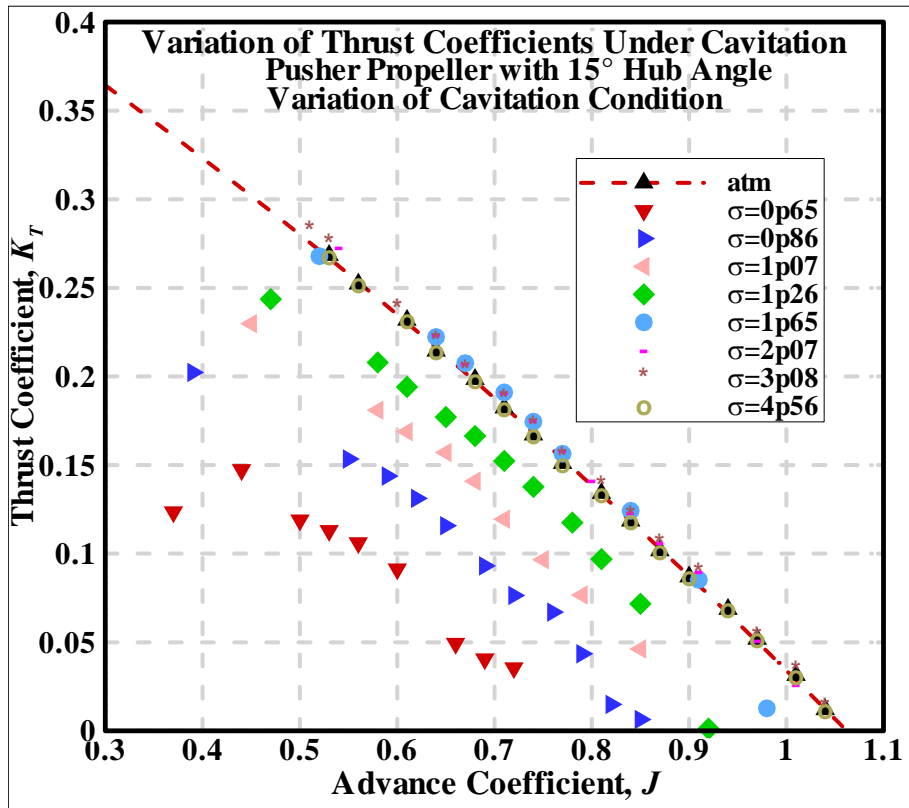


Figure 4-5. K_T of the propeller, Push+15° at different σ_n . $T_W=19.5^\circ (\pm 0.5^\circ)$; $\alpha/\alpha_s=0.2\sim 0.35$.

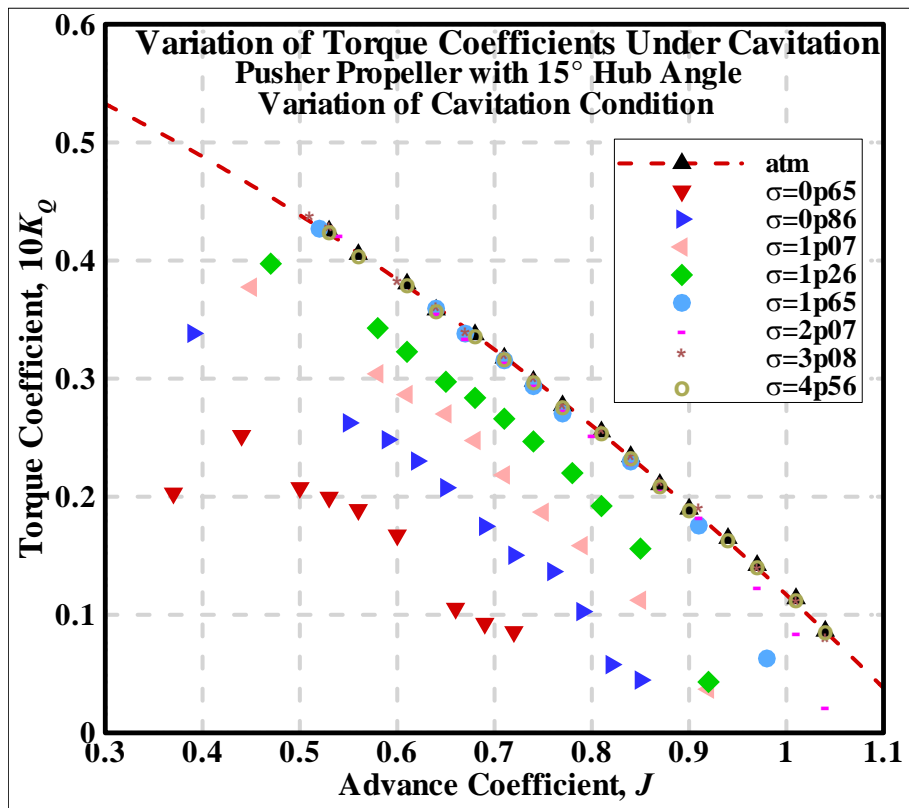


Figure 4-6. K_Q of the propeller, Push+15° at different σ_n . $T_W=19.5^\circ (\pm 0.5^\circ)$; $\alpha/\alpha_s=0.2\sim 0.35$.

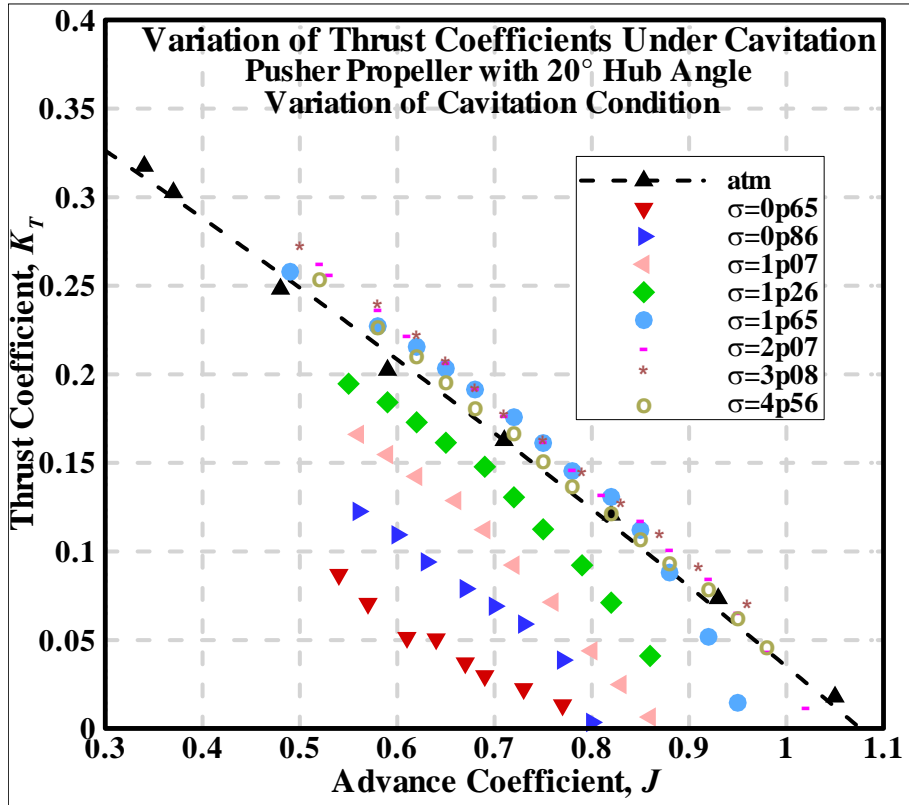


Figure 4-7. K_T of the propeller, Push+20° at different σ_n . $T_W=19.5^\circ (\pm 0.5^\circ)$; $\alpha/\alpha_s=0.2\sim 0.35$.

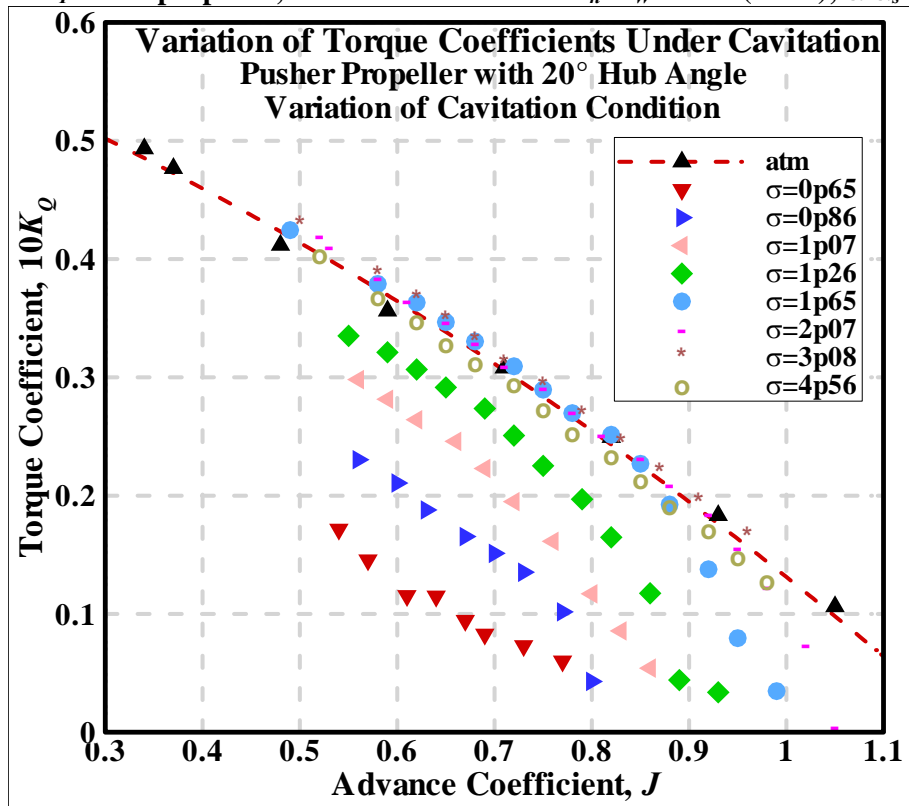


Figure 4-8. K_Q of the propeller, Push+20° at different σ_n . $T_W=19.5^\circ (\pm 0.5^\circ)$; $\alpha/\alpha_s=0.2\sim 0.35$.

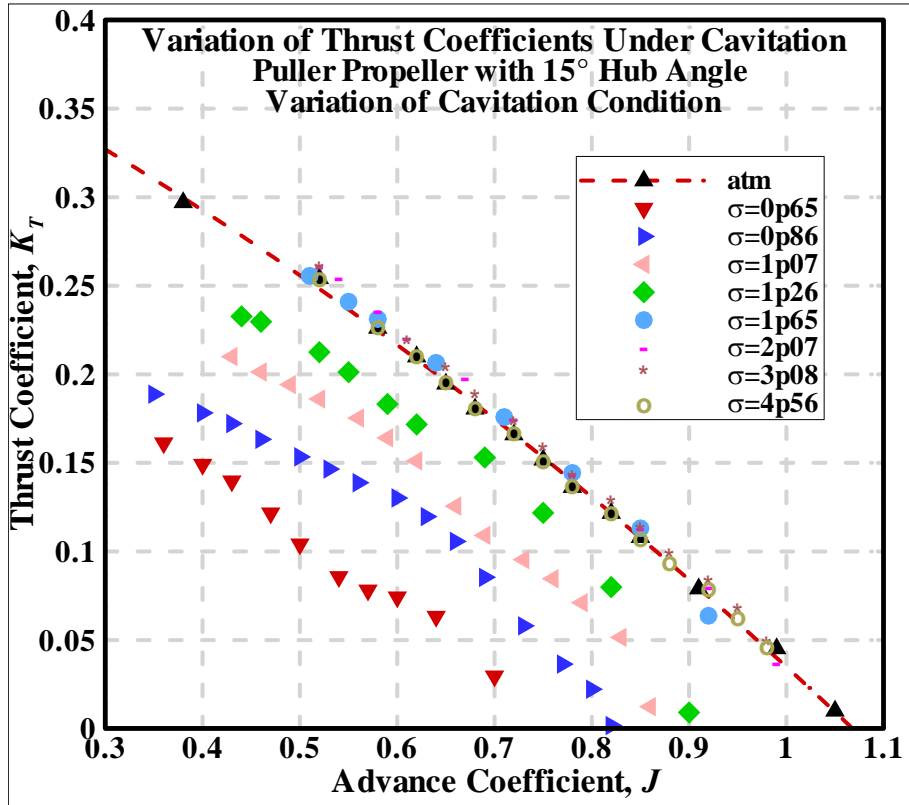


Figure 4-9. K_T of the propeller, Pull-15° at different σ_n . $T_W=19.5^\circ (\pm 0.5^\circ)$; $\alpha/\alpha_s=0.2\sim 0.35$.

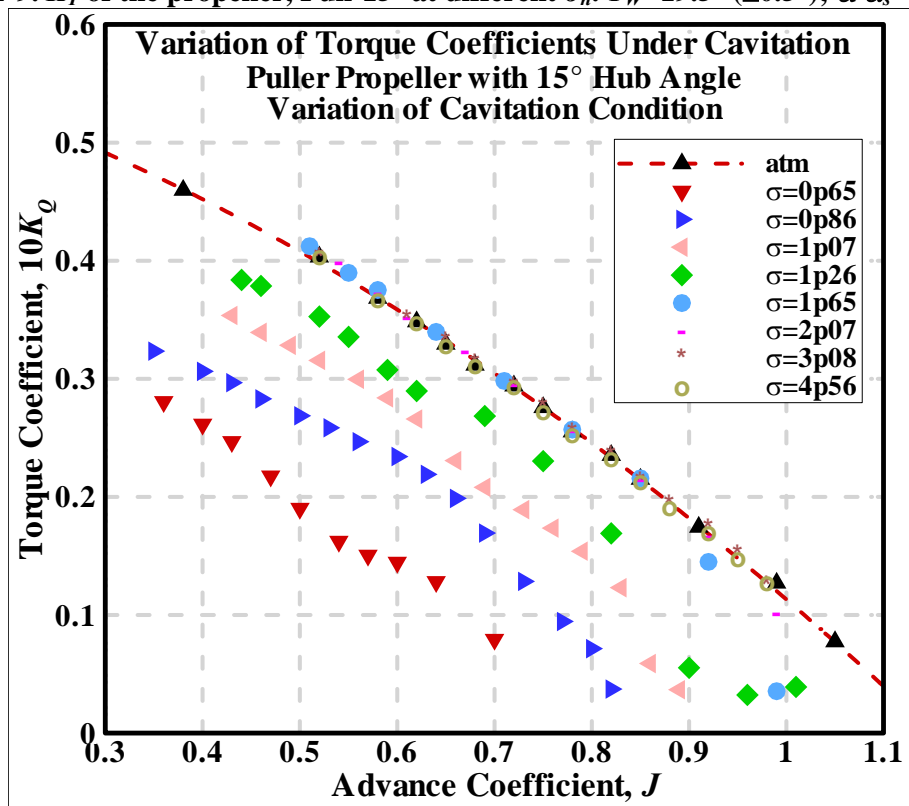


Figure 4-10. K_Q of the propeller, Pull-15° at different σ_n . $T_W=19.5^\circ (\pm 0.5^\circ)$; $\alpha/\alpha_s=0.2\sim 0.35$.

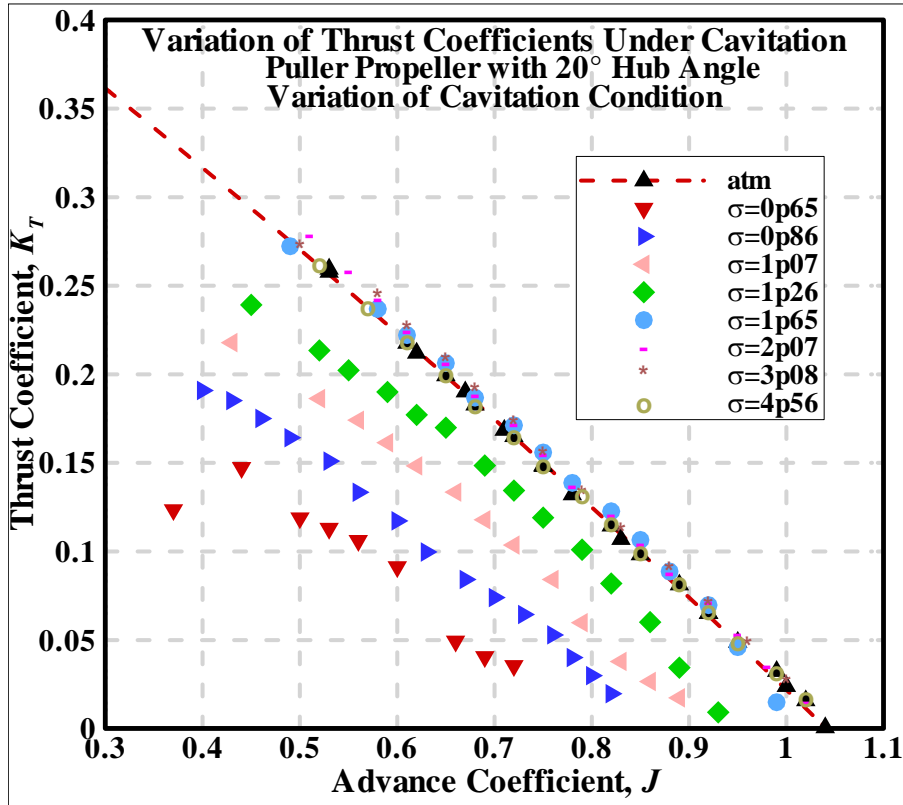


Figure 4-11. K_T of the propeller, Pull-20° at different σ_n . $T_W=19.5^\circ (\pm 0.5^\circ)$; $\alpha/\alpha_s=0.2\sim 0.35$.

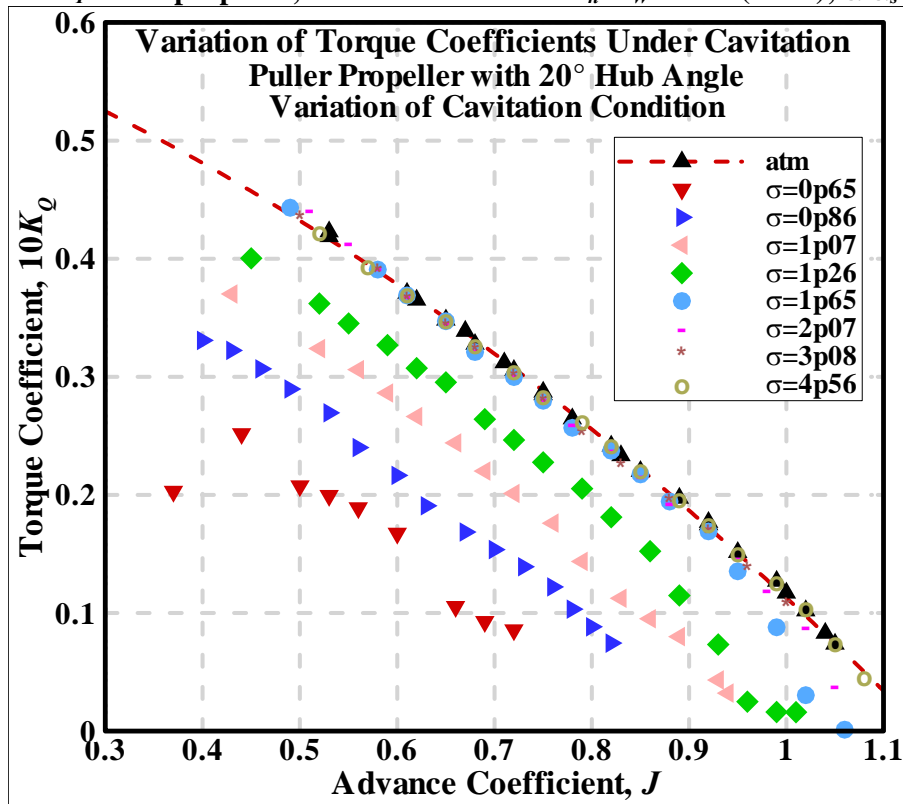


Figure 4-12. K_Q of the propeller, Pull-20° at different σ_n . $T_W=19.5^\circ (\pm 0.5^\circ)$; $\alpha/\alpha_s=0.2\sim 0.35$.

4-2. Reynolds Number Effects:

For the prediction of the performance of a full-scale propeller based on model performance, it is very important that the tests reduce *Reynolds Number* effects to minimum. The tests conducted at high *Reynolds Number* (over 1 million) ensure that any adverse effect of laminar flow (dynamic stall of the blades) over the propellers is avoided. The *Reynolds Number*, $Re_{0.7R}$ for the model propellers is calculated, based on ITTC recommendation in the following:

$$Re_{0.7R} = \frac{c_{0.7R} \sqrt{(0.7\pi nD)^2 + V_A^2}}{\nu} \quad (4.1)$$

where, $c_{0.7R}$ is the local chordlength at 0.7R. R is the radius of the propeller, V_A is the propeller advance speed, ν is the kinematic viscosity of fluid, which is a function of temperature. The tests were carried out at the following three rotational speeds having *Reynolds Numbers* greater than the ITTC recommended critical value of 1 million (Jessup *et al.* 2002).

Table 4-3. Calculation of Reynolds Number for three different propeller rps.

D	$c_{0.7R} / D$ (m)	V_A m/s	n rps	ν (m ² /s)	$Re_{0.7R}$
0.27	0.4622	2.50	15	1.04E-06	1.11E+06
0.27	0.4622	3.00	15	1.04E-06	1.13E+06
0.27	0.4622	3.50	15	1.04E-06	1.15E+06
0.27	0.4622	4.00	15	1.04E-06	1.17E+06
0.27	0.4622	4.50	15	1.04E-06	1.20E+06
0.27	0.4622	5.00	15	1.04E-06	1.23E+06
0.27	0.4622	5.50	15	1.04E-06	1.26E+06
0.27	0.4622	6.00	15	1.04E-06	1.29E+06
0.27	0.4622	6.50	15	1.04E-06	1.32E+06
0.27	0.4622	7.00	15	1.04E-06	1.36E+06
0.27	0.4622	7.50	15	1.04E-06	1.40E+06
0.27	0.4622	8.00	15	1.04E-06	1.44E+06
0.27	0.4622	2.50	20	1.04E-06	1.46E+06
0.27	0.4622	3.00	20	1.04E-06	1.47E+06
0.27	0.4622	3.50	20	1.04E-06	1.49E+06
0.27	0.4622	4.00	20	1.04E-06	1.50E+06
0.27	0.4622	4.50	20	1.04E-06	1.52E+06
0.27	0.4622	5.00	20	1.04E-06	1.55E+06
0.27	0.4622	5.50	20	1.04E-06	1.57E+06
0.27	0.4622	6.00	20	1.04E-06	1.60E+06
0.27	0.4622	6.50	20	1.04E-06	1.62E+06
0.27	0.4622	7.00	20	1.04E-06	1.65E+06
0.27	0.4622	7.50	20	1.04E-06	1.69E+06

0.27	0.4622	8.00	20	1.04E-06	1.72E+06
0.27	0.4622	2.50	25	1.04E-06	1.81E+06
0.27	0.4622	3.00	25	1.04E-06	1.82E+06
0.27	0.4622	3.50	25	1.04E-06	1.83E+06
0.27	0.4622	4.00	25	1.04E-06	1.84E+06
0.27	0.4622	4.50	25	1.04E-06	1.86E+06
0.27	0.4622	5.00	25	1.04E-06	1.88E+06
0.27	0.4622	5.50	25	1.04E-06	1.90E+06
0.27	0.4622	6.00	25	1.04E-06	1.92E+06
0.27	0.4622	6.50	25	1.04E-06	1.94E+06
0.27	0.4622	7.00	25	1.04E-06	1.97E+06
0.27	0.4622	7.50	25	1.04E-06	2.00E+06
0.27	0.4622	8.00	25	1.04E-06	2.02E+06

The basic performance tests under cavitating conditions for the four propellers were done at shaft speeds of 25 rps, which corresponds to a *Reynolds Number* of 2.018×10^6 . This high propeller rotational speed was selected in order to get low cavitation number (see equation 3-1). Several additional tests were conducted at the design cavitation number ($\sigma_{design}=3.0$) to study the *Reynolds Number* effects, if any. The experimental *Reynolds Number* was changed by changing the propeller rotational speeds. Tests were done at shaft speeds of 15 rps and 20 rps and the measured performance was compared to the 25 rps tests at the design cavitation number. The results are presented in Figures 4-13 to 4-16.

In the Figures 4-13 to 4-16, it is observed that for all the four propellers the measured performance at the design cavitation number ($\sigma_{design}=3.0$) at 20 rps were almost the same as that of the 25 rps (the efficiencies were within 3%), while very narrow difference in performance are seen between that of 20 rps and 15 rps (the efficiencies were within 10%). This indicated that *Reynolds Number* effects were very limited and could be neglected when the propeller operation speed exceed 20 rps. The model propellers were big enough (270 mm diameter) to avoid any *Reynolds Number* effect (similar flow condition over the surface of the blades between the model scale and the full scale) when they were operating at 20 rps or higher.

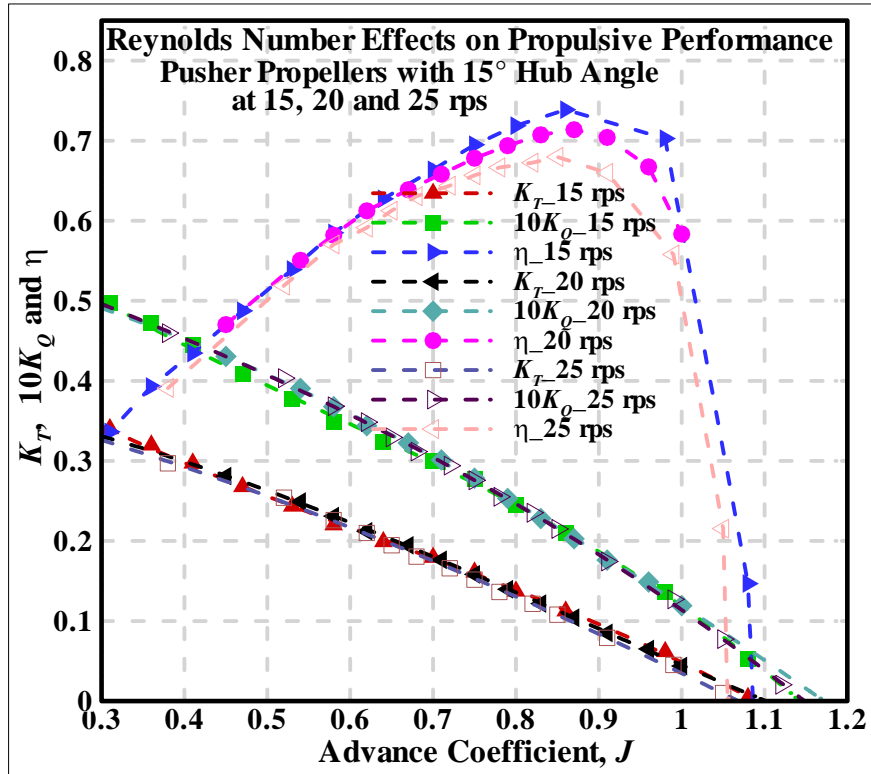


Figure 4-13. Performance of the propeller, Push+15° at $\sigma_{design}=3.0$, at three different *Reynolds Numbers* (three different rps, 15, 20, 25). $T_W=19.5^\circ (\pm 1)$; $\alpha/\alpha_s=0.2\sim 0.35$.

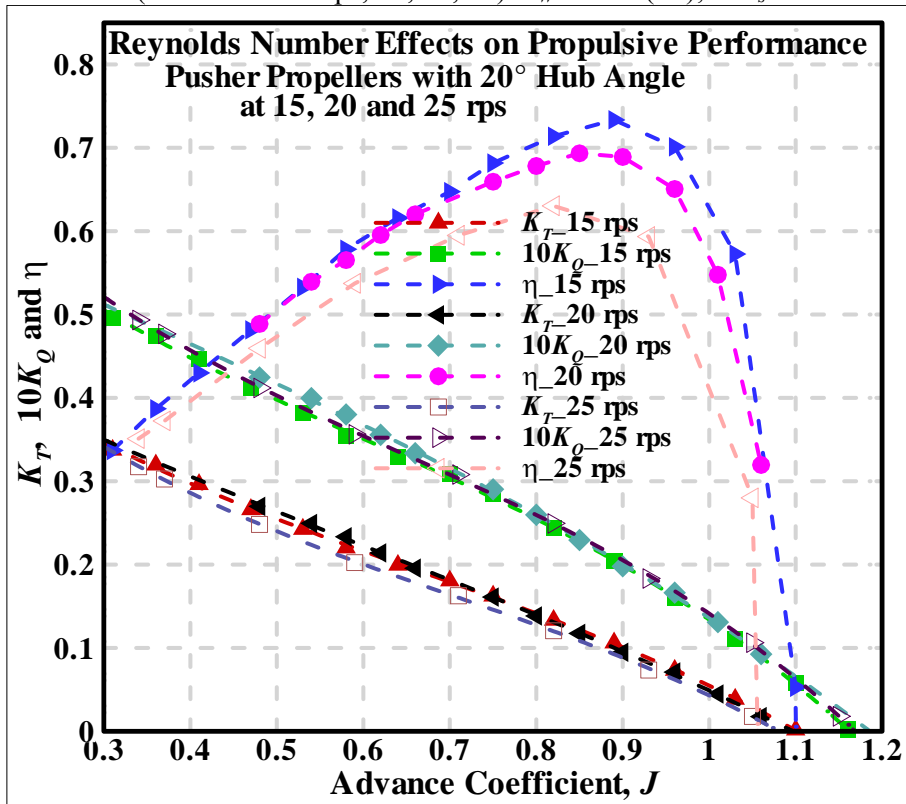


Figure 4-14. Performance of the propeller, Push+20° at $\sigma_{design}=3.0$, at three different *Reynolds Numbers* (three different rps, 15, 20, 25). $T_W=19.5^\circ (\pm 1)$; $\alpha/\alpha_s=0.2\sim 0.35$.

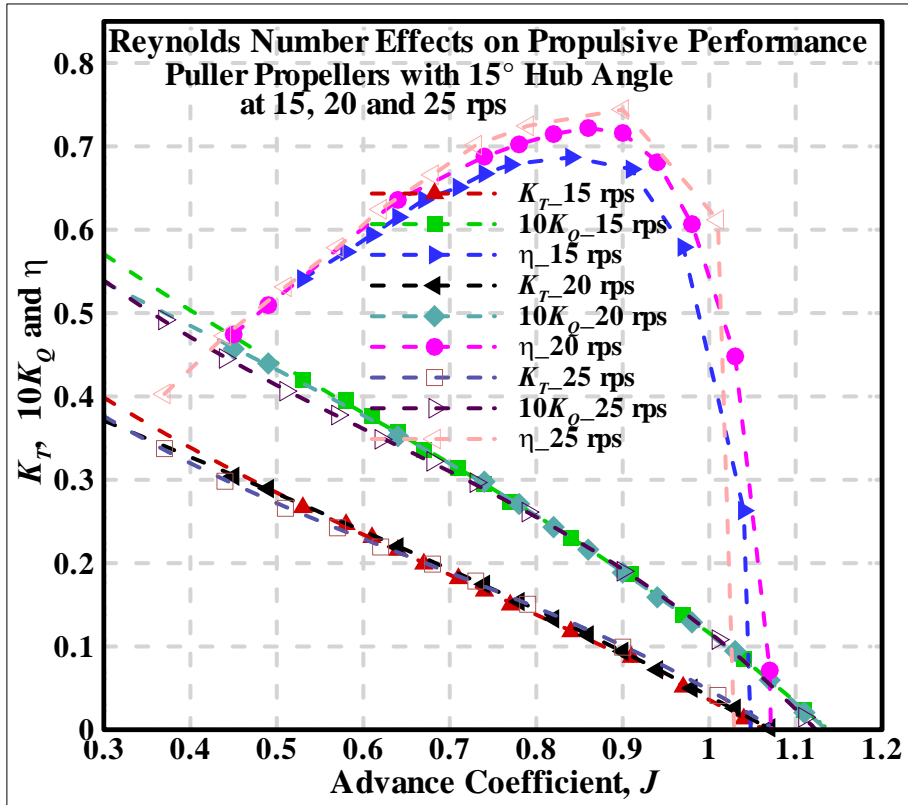


Figure 4-15. Performance of the propeller, Pull-15° at $\sigma_{design}=3.0$, at three different *Reynolds Numbers* (three different rps, 15, 20, 25). $T_W=19.5^\circ (\pm 1)$; $\alpha/\alpha_s=0.2\sim 0.35$.

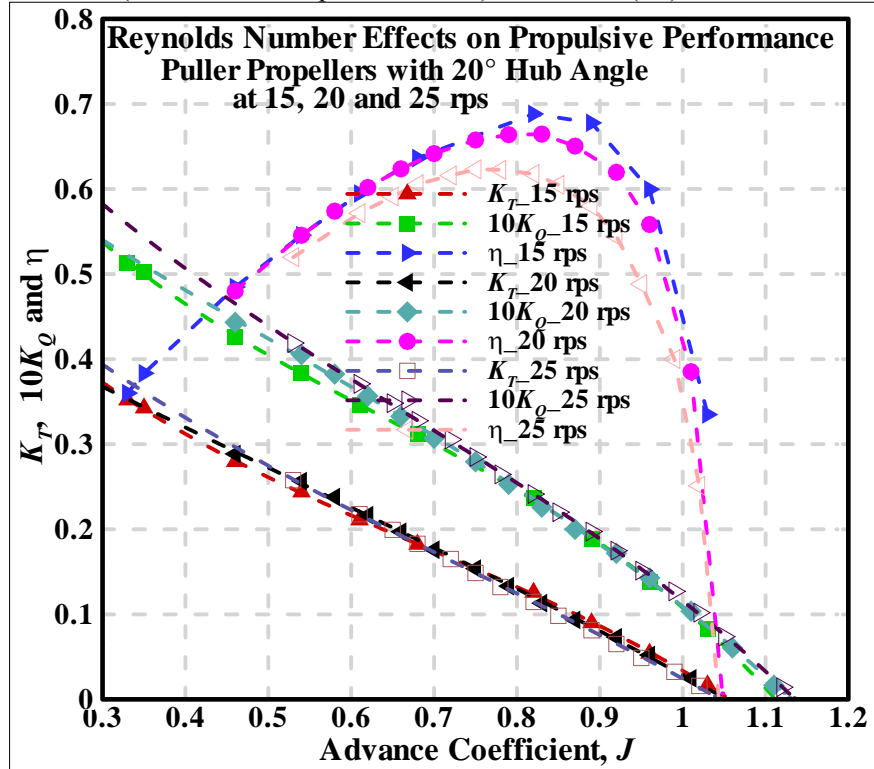


Figure 4-16. Performance of the propeller, Pull-20° at $\sigma_{design}=3.0$, at three different *Reynolds Numbers* (three different rps, 15, 20, 25). $T_W=19.5^\circ (\pm 1)$; $\alpha/\alpha_s=0.2\sim 0.35$.

4-3. Hub Taper Angle Effects on Performance

The effect of hub taper angle on propulsive performance under cavitation can be studied by analyzing the results in terms of K_T , K_Q and J for different cavitation number, α_n . Comparison of performance of two propellers with 15° and 20° hub taper angles in either pusher or puller configuration reveals the effect of hub taper angle on performance. Figures 4-17(a) to 4-17(h) provide comparisons between the propellers Push+15° and Push+20° and Figures 4-18(a) to 4-18(h) provide comparisons between the propellers Pull-15° and Pull-20°.

Comparison between the push+15 and Push+20 propellers (Figures 4-17(a) to 4-17(h)) show that, increasing the hub taper angle increased the torque, and this effect increased with advance coefficient. For thrust, increasing the taper angle also increased the thrust but not with the same magnitude as torque coefficient and the increase is more obvious at higher advance coefficient. The net effect on the propeller efficiency was that the efficiency decreased for larger hub angles and the effect was more pronounced for higher advance coefficient. The similar effects were observed for all the cavitation conditions except at low cavitation number ($\alpha_n=1.0$) where the comparison was not very obvious. This inconsistency in data might result from the unusual tunnel behavior (too much noise and vibration from the tunnel) in the operating condition.

Comparison between the pull-15 and Pull-20 propellers (Figures 4-18(a) to 4-18(h)) show that, increasing the hub taper angle increased the torque, and this effect increased with increasing advance coefficient. For thrust, increasing the taper angle also increased the thrust but not with the same magnitude as torque coefficient and the increase is more obvious at lower advance coefficient. The net effect on the propeller efficiency was that the efficiency decreased for larger hub angles and the difference in efficiency got larger with increasing advance coefficient. The similar effects were observed for all the cavitation conditions except at low cavitation number ($\alpha_n=1.0$) where the comparison was not very obvious. This inconsistency in data might result from the unusual tunnel behavior (too much noise and vibration from the tunnel) in the operating condition.

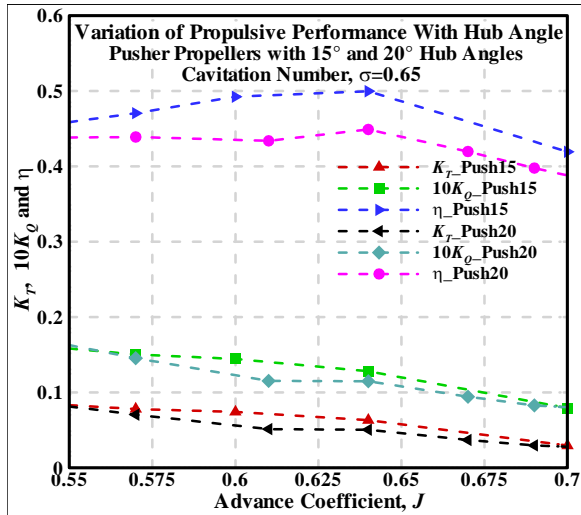


Figure 4-17 (a). Comparison of K_T and K_Q of the Push+15° and the push+20° propellers at $\sigma=0.65$.

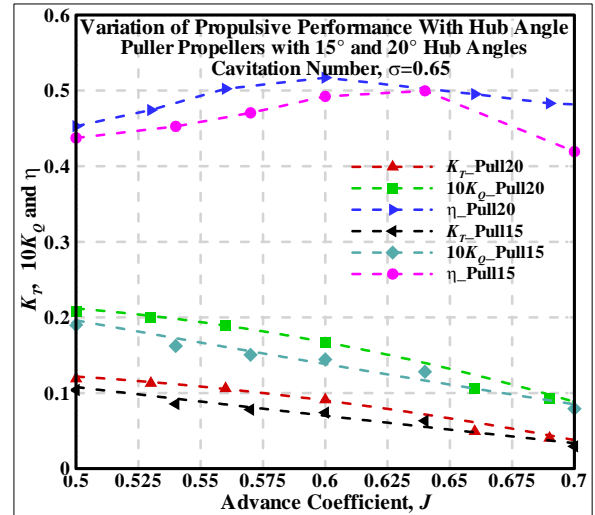


Figure 4-18 (a). Comparison of K_T and K_Q of the Pull-15° and the pull-20° propellers at $\sigma=0.65$.

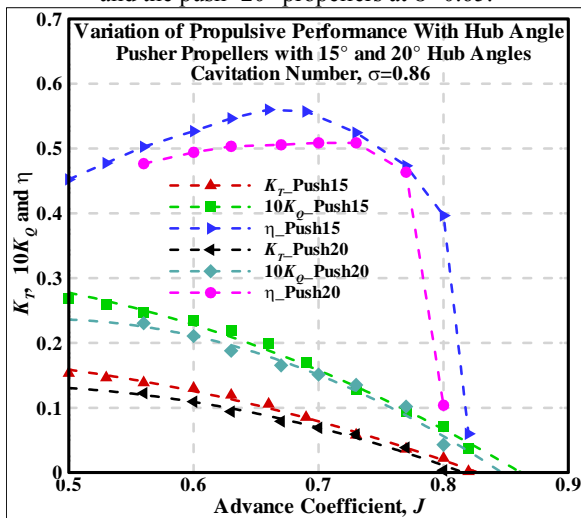


Figure 4-17 (b). Comparison of K_T and K_Q of the Push+15° and the push+20° propellers at $\sigma=0.86$.

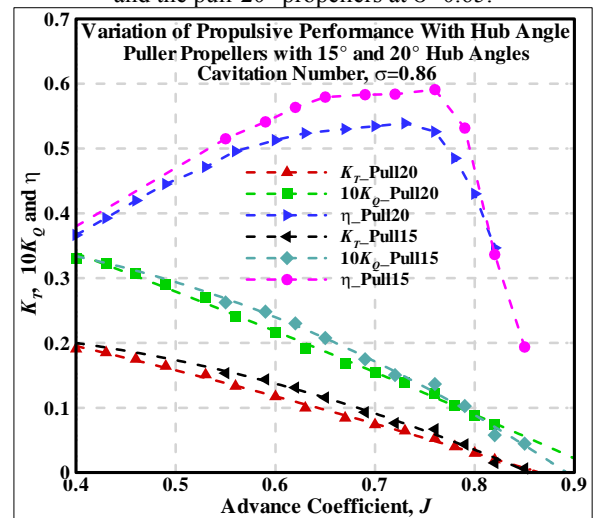


Figure 4-18 (b). Comparison of K_T and K_Q of the Pull-15° and the pull-20° propellers at $\sigma=0.86$.

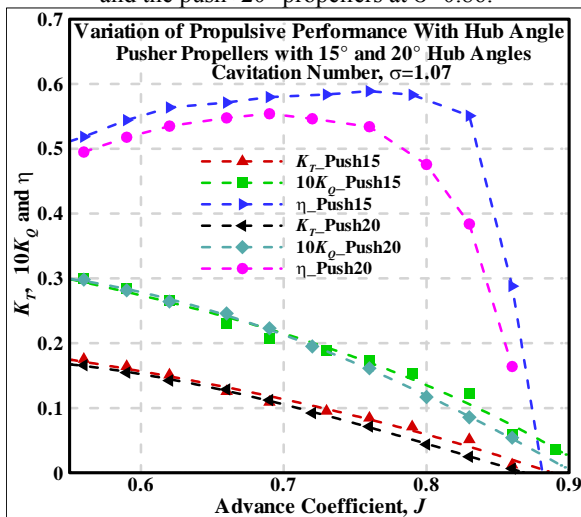


Figure 4-17 (c). Comparison of K_T and K_Q of the Push+15° and the push+20° propellers at $\sigma=1.07$.

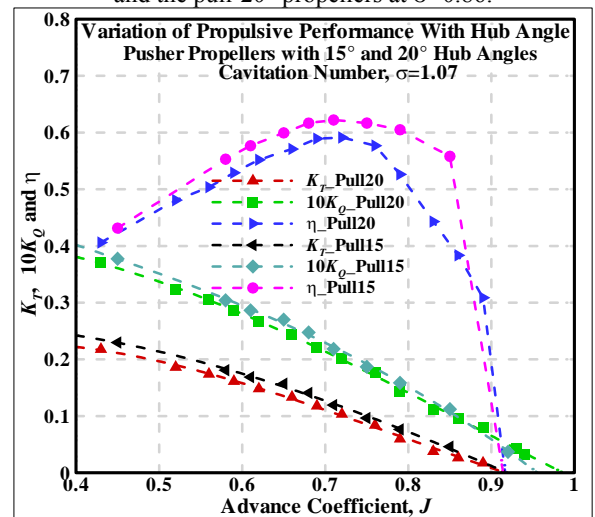


Figure 4-18 (c). Comparison of K_T and K_Q of the Pull-15° and the pull-20° propellers at $\sigma=1.07$.

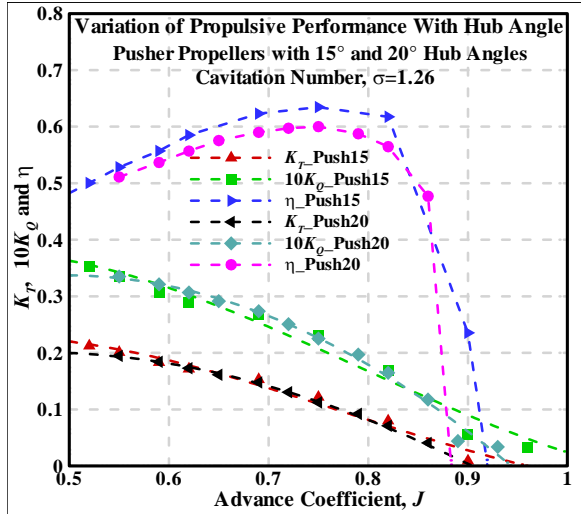


Figure 4-17 (d). Comparison of K_T and K_Q of the Push+15° and the push+20° propellers at $\sigma=1.26$.

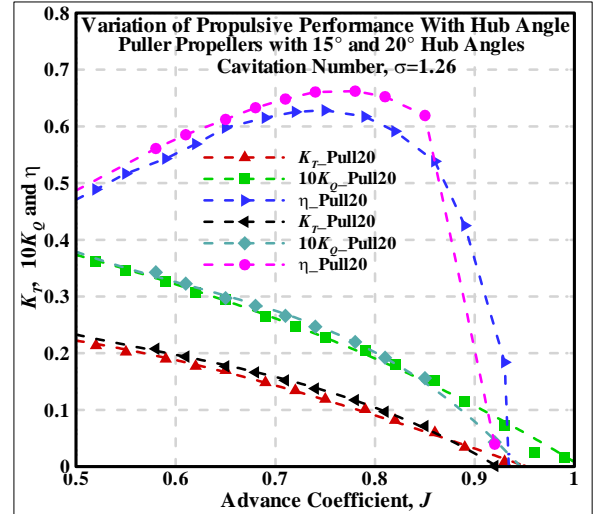


Figure 4-18 (d). Comparison of K_T and K_Q of the Pull-15° and the pull-20° propellers at $\sigma=1.26$.

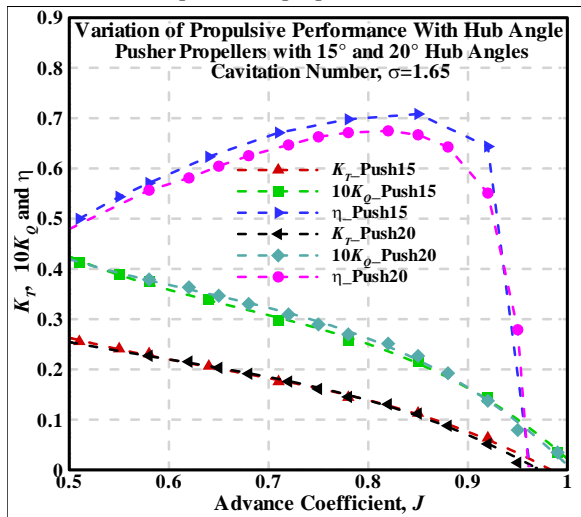


Figure 4-17 (e). Comparison of K_T and K_Q of the Push+15° and the push+20° propellers at $\sigma=1.65$.

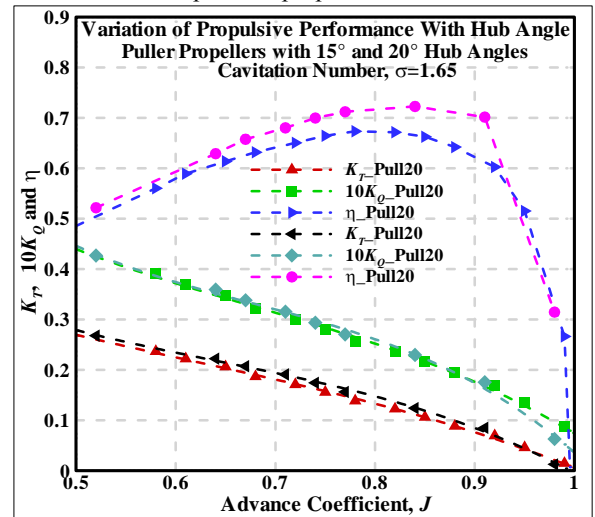


Figure 4-18 (e). Comparison of K_T and K_Q of the Pull-15° and the pull-20° propellers at $\sigma=1.65$.

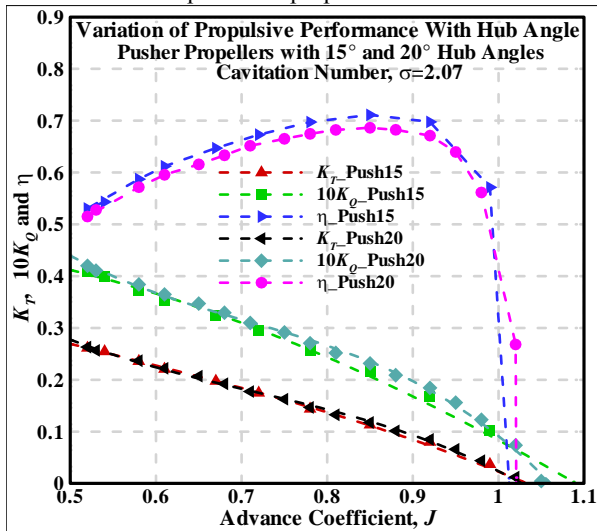


Figure 4-17 (f). Comparison of K_T and K_Q of the Push+15° and the push+20° propellers at $\sigma=2.07$.

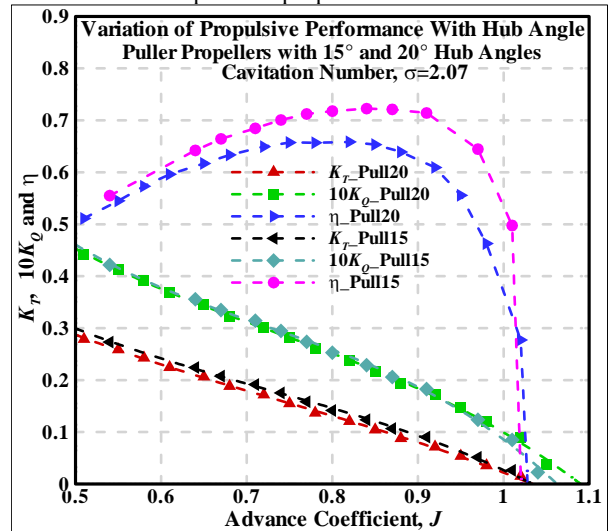


Figure 4-18 (f). Comparison of K_T and K_Q of the Pull-15° and the pull-20° propellers at $\sigma=2.07$.

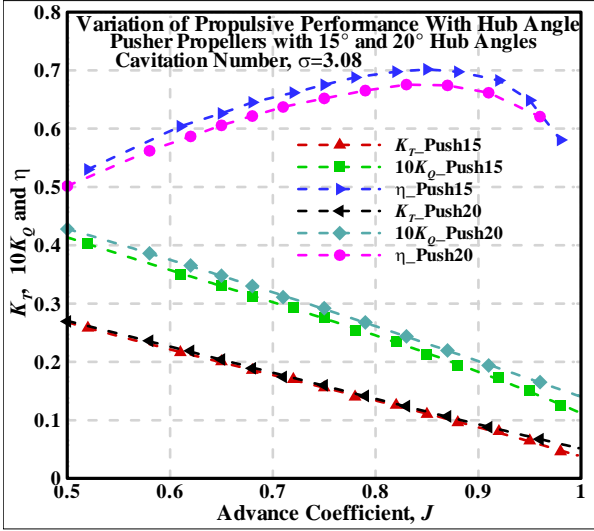


Figure 4-17 (g). Comparison of K_T and K_Q of the Push+15° and the push+20° propellers at $\sigma=3.08$.

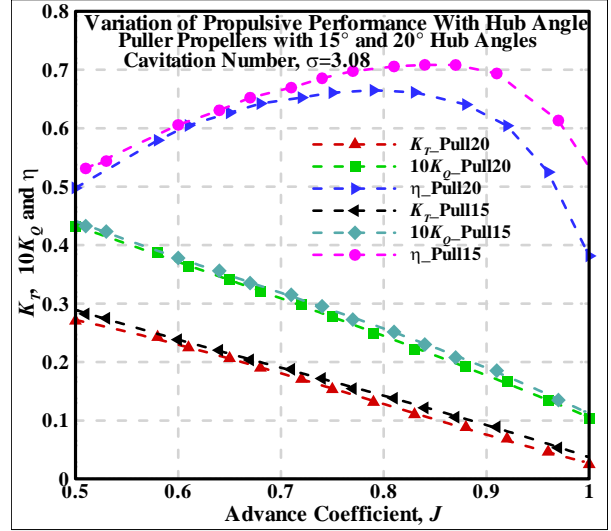


Figure 4-18 (g). Comparison of K_T and K_Q of the Pull-15° and the pull-20° propellers at $\sigma=3.08$.

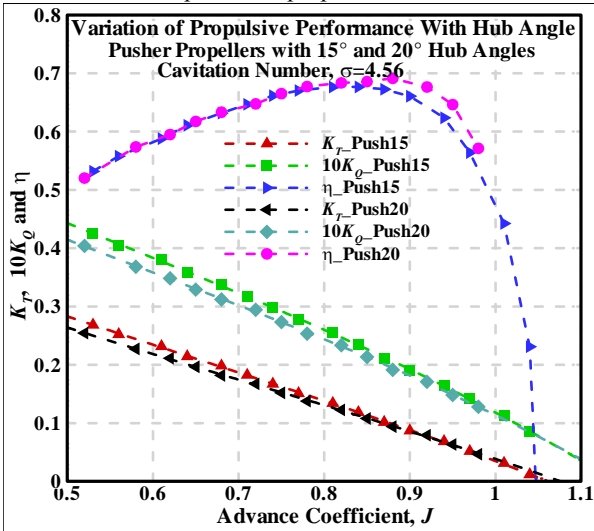


Figure 4-17 (h). Comparison of K_T and K_Q of the Push+15° and the push+20° propellers at $\sigma=4.56$.

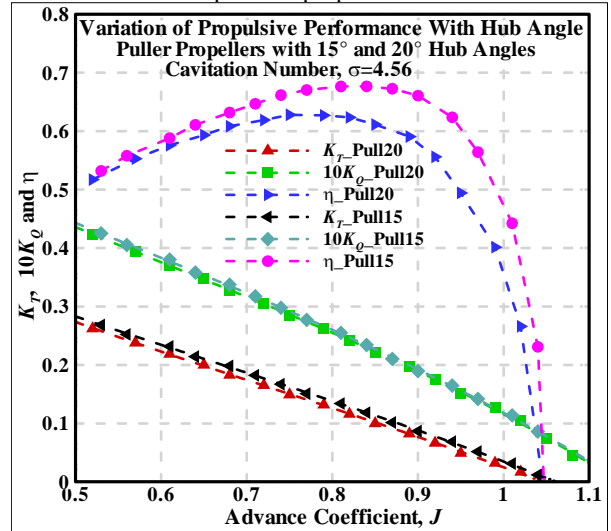


Figure 4-18 (h). Comparison of K_T and K_Q of the Pull-15° and the pull-20° propellers at $\sigma=4.56$.

4-4. Comparison of Push and Pull Configurations

One of the main objectives of this experimental study was to investigate the dependency of propulsive performance on the mode of operation of the podded propellers (propeller only case) for which that propeller was designed: push or pull at different cavitating conditions. To this end, comparisons of the performance of push configurations relative to their pull counterparts are presented for both hub angles and are given for all the cavitation numbers experiments. Comparison of performance of two propellers with same hub taper angle but different configurations (pusher and puller) reveals the effect of configuration on performance. Figures 4-19(a) to 4-19(i) provide comparisons between the propellers

Push+15° and Pull-15° and Figures 4-20(a) to 4-20(i) provide comparisons between the propellers Push+20° and Pull-20°.

Based on the Figures 4-19(a) to 4-19(i), it can be seen that the push configuration propellers consistently had lower torque and thrust coefficients than their puller counterparts tested under the same cavitation conditions. The increase in thrust and torque for the puller propellers as compared to those of the pusher ones were more obvious at lower advance coefficient values. The overall effect on the propeller efficiency is a slight decrease of efficiency for the pusher propellers, particularly for the lightly loaded conditions.

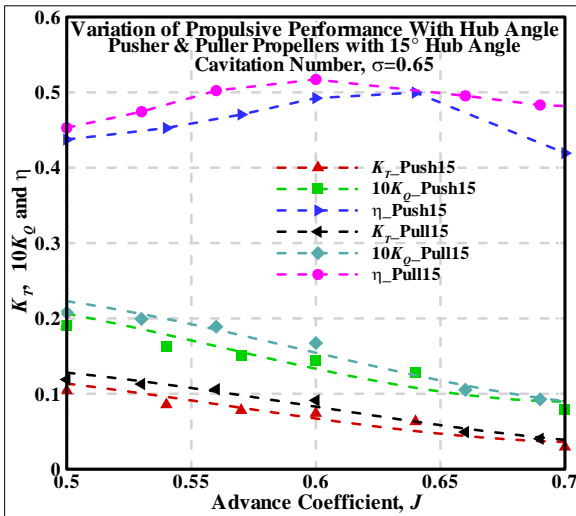


Figure 4-19 (a). Comparison of K_T and K_Q of the Push+15° and the pull-15° propellers at $\sigma=0.65$.

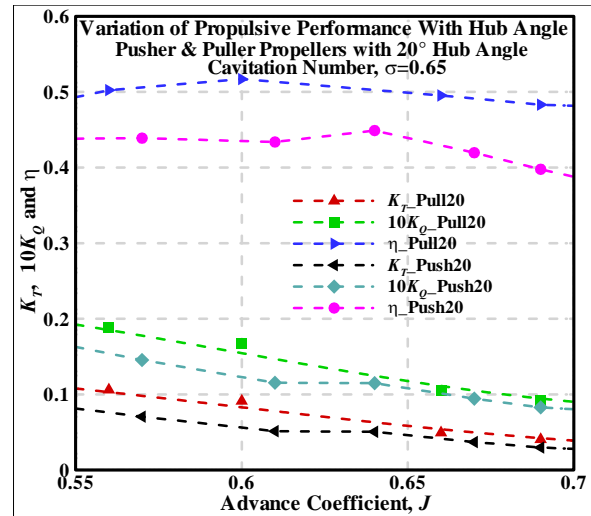


Figure 4-20 (a). Comparison of K_T and K_Q of the Pull-20° and the push+20° propellers at $\sigma=0.65$.

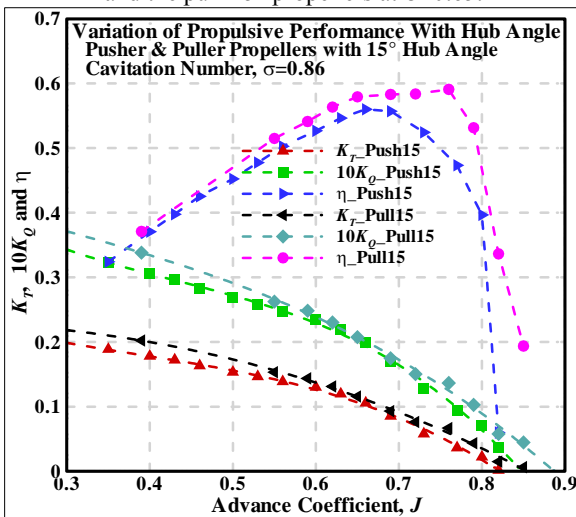


Figure 4-19 (b). Comparison of K_T and K_Q of the Push+15° and the pull-15° propellers at $\sigma=0.86$.

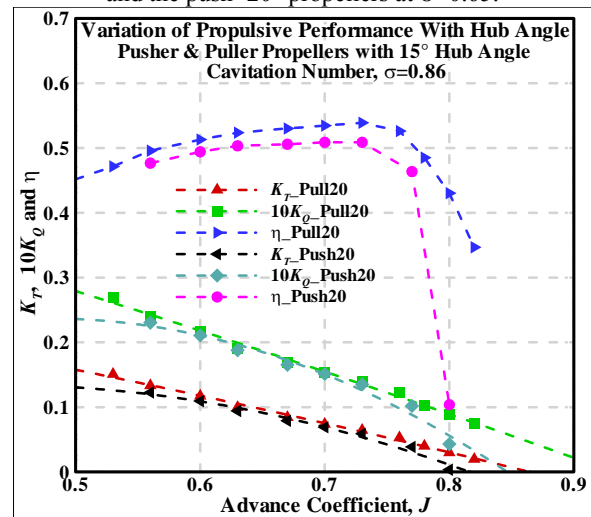


Figure 4-20 (b). Comparison of K_T and K_Q of the Pull-20° and the push+20° propellers at $\sigma=0.86$.

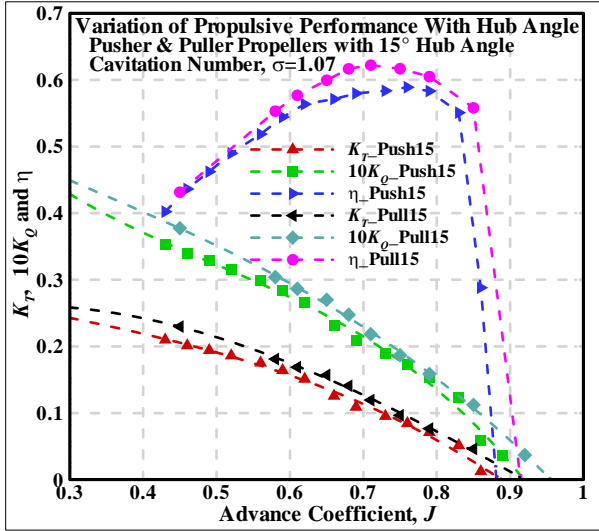


Figure 4-19 (c). Comparison of K_T and K_Q of the Push+15° and the pull-15° propellers at $\sigma=1.07$.

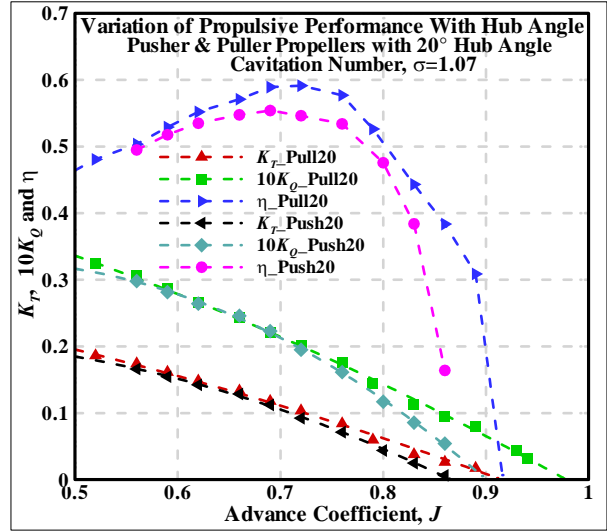


Figure 4-20 (c). Comparison of K_T and K_Q of the Pull-20° and the push+20° propellers at $\sigma=1.07$.

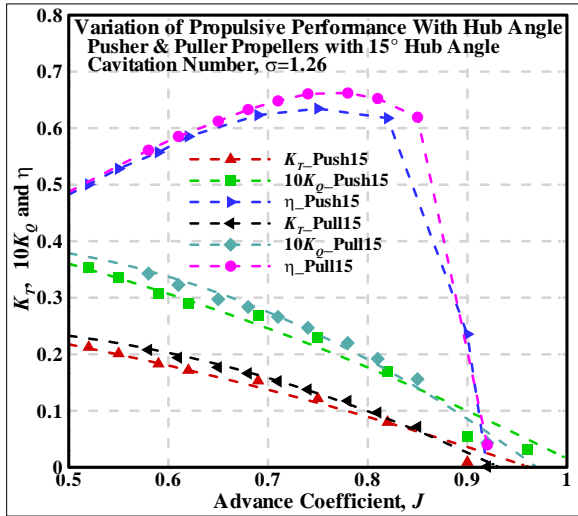


Figure 4-19 (d). Comparison of K_T and K_Q of the Push+15° and the pull-15° propellers at $\sigma=1.26$.

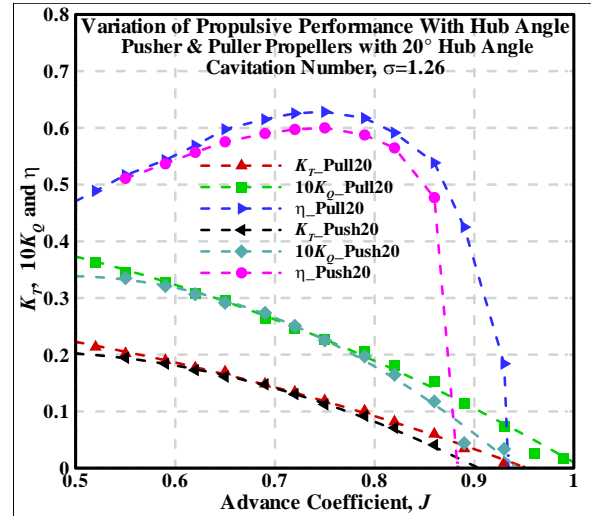


Figure 4-20 (d). Comparison of K_T and K_Q of the Pull-20° and the push+20° propellers at $\sigma=1.26$.

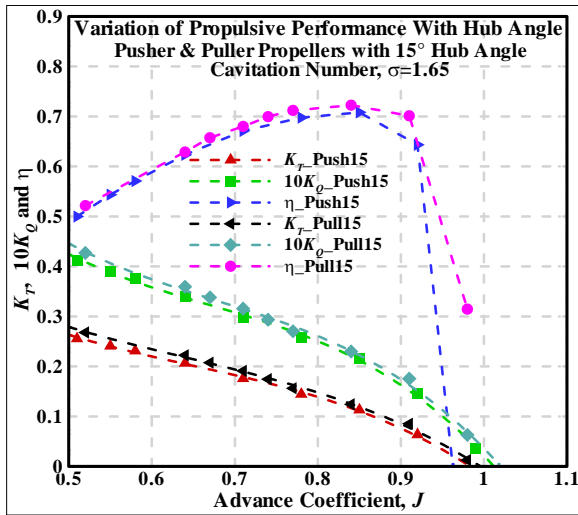


Figure 4-19 (e). Comparison of K_T and K_Q of the Push+15° and the pull-15° propellers at $\sigma=1.65$.

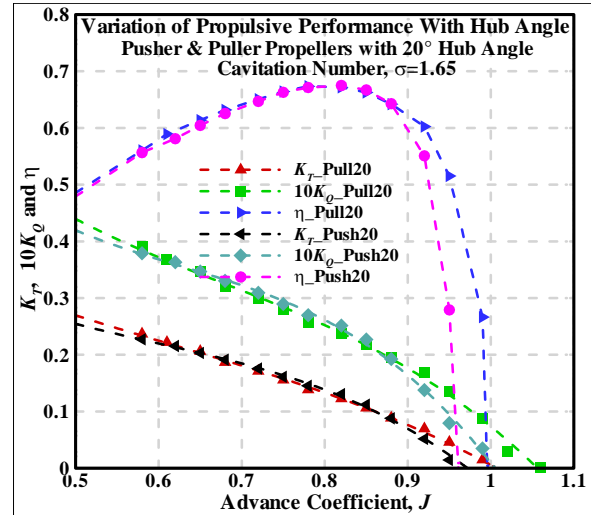


Figure 4-20 (e). Comparison of K_T and K_Q of the Pull-20° and the push+20° propellers at $\sigma=1.65$.

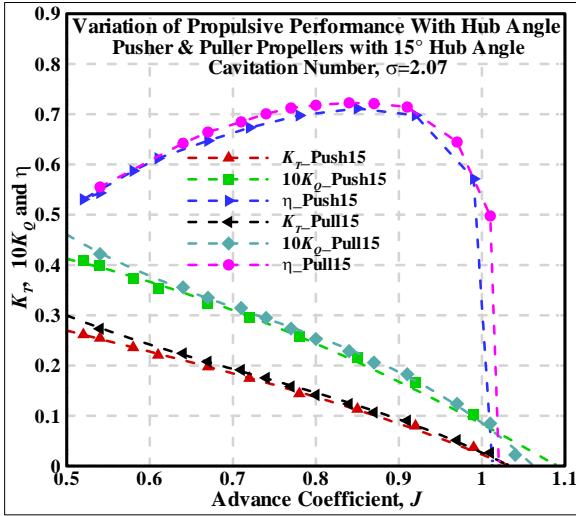


Figure 4-19 (f). Comparison of K_T and K_Q of the Push+15° and the pull-15° propellers at $\sigma=2.07$.

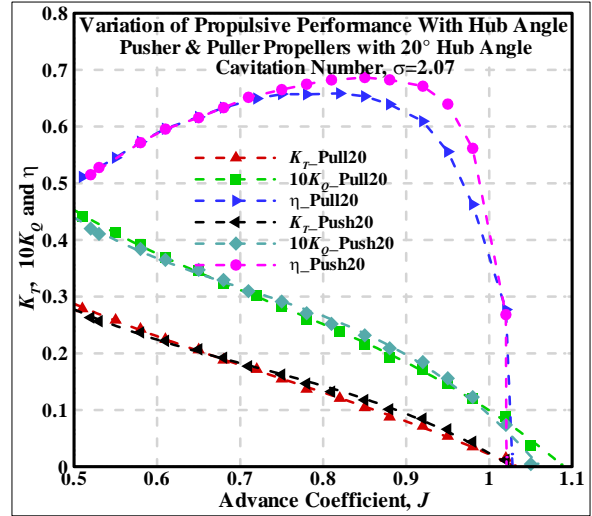


Figure 4-20 (f). Comparison of K_T and K_Q of the Pull-20° and the push+20° propellers at $\sigma=2.07$.

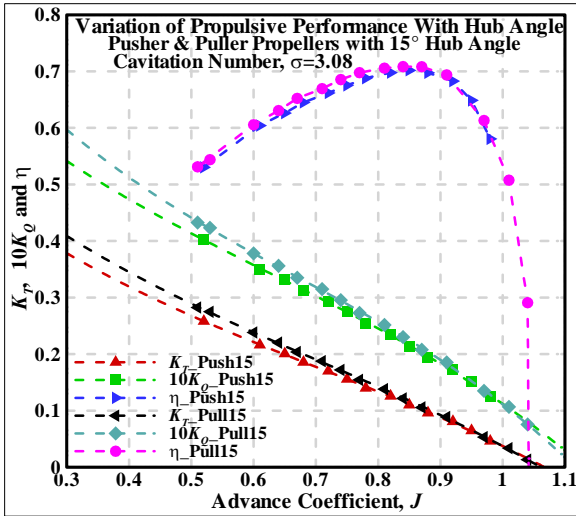


Figure 4-19 (g). Comparison of K_T and K_Q of the Push+15° and the pull-15° propellers at $\sigma=3.08$.

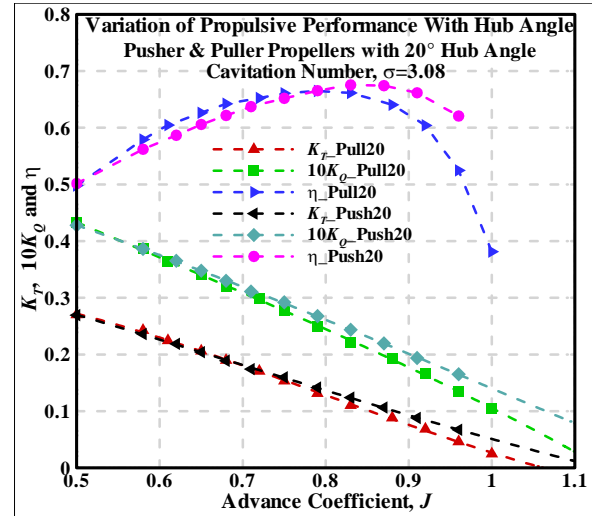


Figure 4-20 (g). Comparison of K_T and K_Q of the Pull-20° and the push+20° propellers at $\sigma=3.08$.

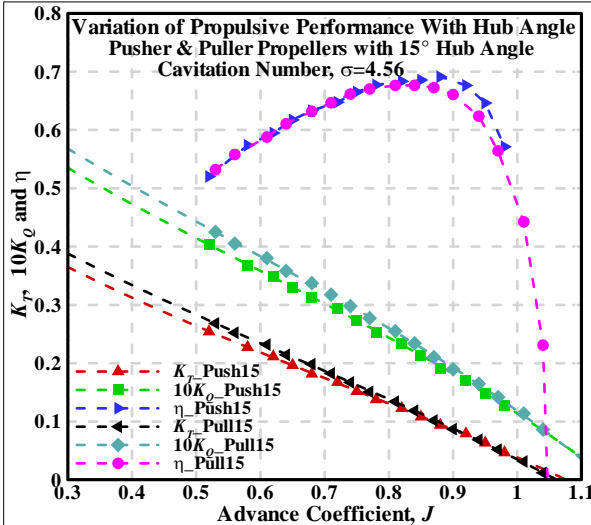


Figure 4-19 (h). Comparison of K_T and K_Q of the Push+15° and the pull-15° propellers at $\sigma=4.56$.

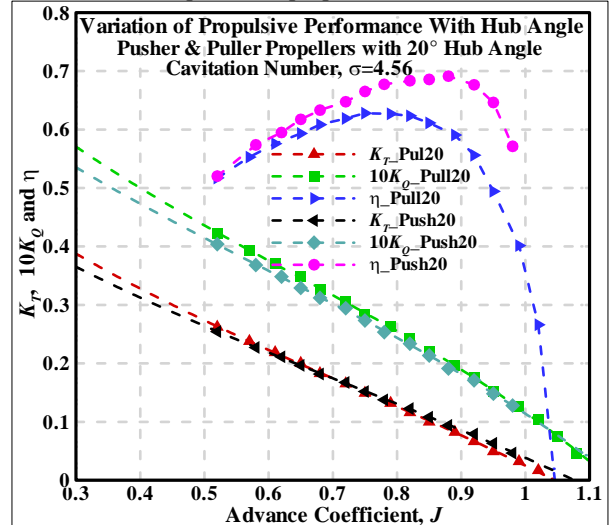


Figure 4-20 (h). Comparison of K_T and K_Q of the Pull-20° and the push+20° propellers at $\sigma=4.56$.

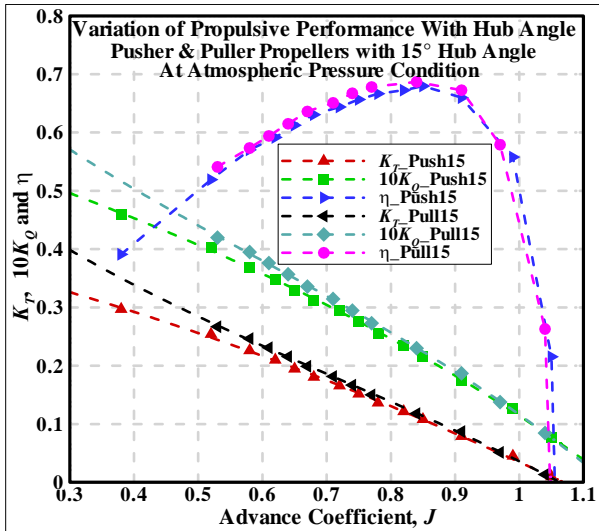


Figure 4-19 (i). Comparison of K_T and K_Q of the Push+15° and the pull-15° propellers at atmospheric pressure.

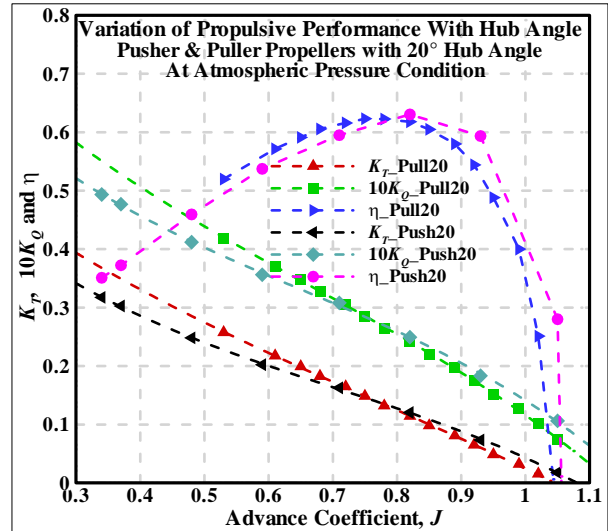


Figure 4-20 (h). Comparison of K_T and K_Q of the Pull-20° and the push+20° propellers at atmospheric pressure.

Figure 4-21 shows the effect of taper angle on thrust coefficient, K_T as the cavitation number increases with three fixed J s. It can be seen from the figure that at all cavitation numbers, the propeller in pull configuration (Pull-15°) produced more thrust than the Push+15° propeller at lower advance coefficient and the difference reduced at increasing advance coefficient (up to J equal to 0.8). At high advance coefficient of 1.0, the two propellers produced almost equal thrust at all cavitating conditions. The figure also shows that for all the cavitation numbers, the difference in K_T for the Pull-15° and Push+15° propellers remains almost same for the three J values. This means the relative thrust produced by the two propellers does not change under cavitation. Similar trend was observed for the torque coefficient at shown in Figure 4-22. It can be seen that the Push+15° propeller consumed more torque than Pull-15° at high advance coefficient of 1.0, whereas the opposite was observed at lower advance coefficients. Figure 4-23 shows the comparison of thrust coefficient of the two propellers with opposite configurations (Push+20° and Pull-20°) as the cavitation number increases with three fixed J s. It can be seen from the figure that at advance coefficient of 0.58, the propeller in pull configuration (Pull-20°) produced more thrust than the Push+20° propeller but at advance coefficient of 0.7 they produced almost equal thrust at all cavitation numbers. However, at advance coefficient of 0.80, the push+20° propeller produced higher thrust when the cavitation number was higher than 1.6. This means when the propeller hub taper angle is high (20° or more) then at moderate and high advance coefficient, the pusher configuration propeller produced more thrust than the puller propellers. Similar trend was observed for the torque coefficient at shown in Figure 4-24. It can be seen that the Push+20° propeller

consumed more torque than Pull-20° at design advance coefficient of 0.8, whereas the opposite was observed at lower advance coefficients.

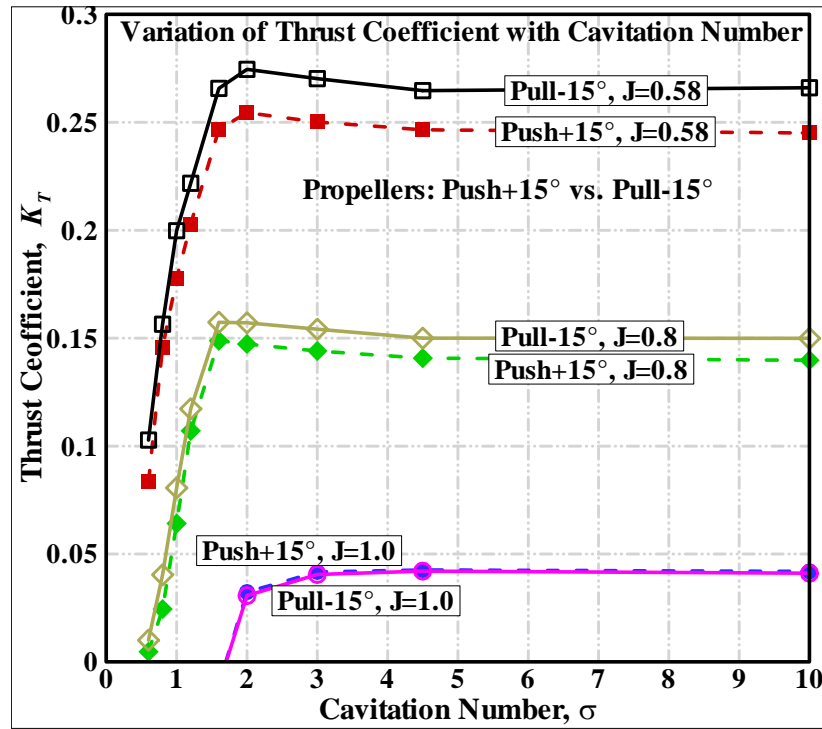


Figure 4-21. Comparison of thrust coefficient (Push+15° and Pull-15° propellers) variation with cavitation number for fixed advance coefficients.

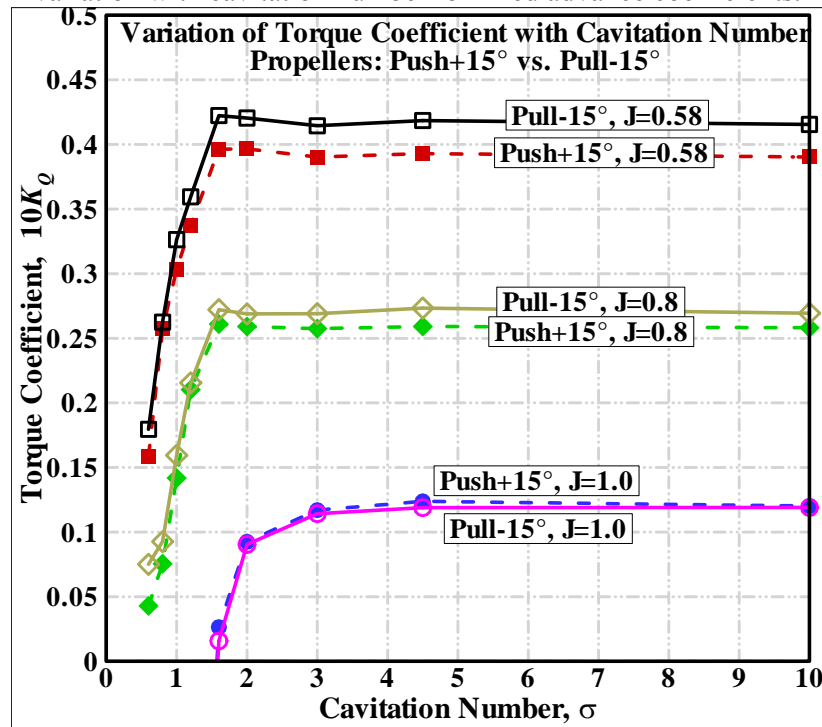


Figure 4-22. Comparison of torque coefficients (Push+15° and Pull-15°) at different cavitation numbers for fixed advance coefficients.

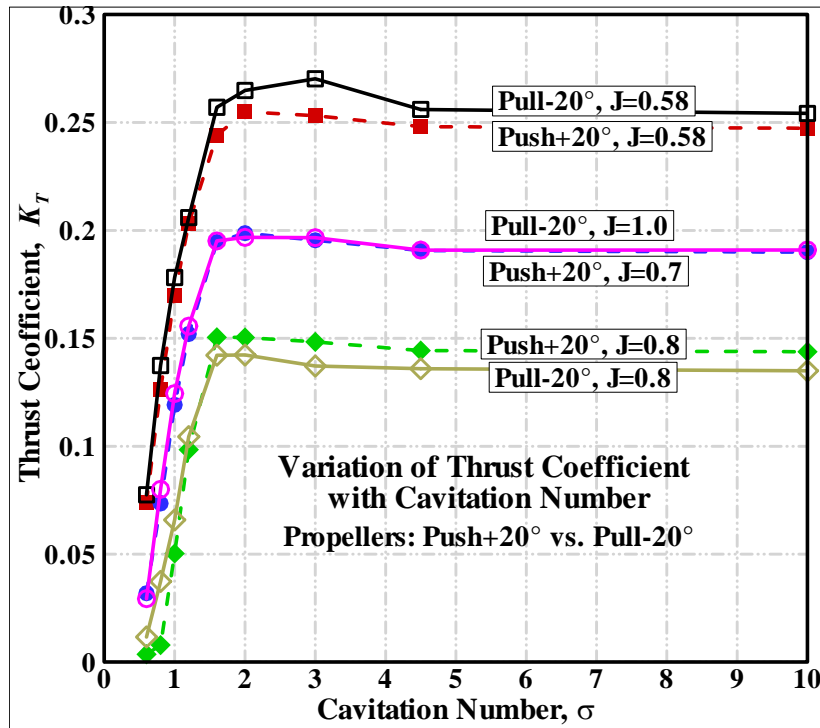


Figure 4-23. Comparison of thrust coefficient (Push+20° and Pull-20° propellers) variation with cavitation number for fixed advance coefficients.

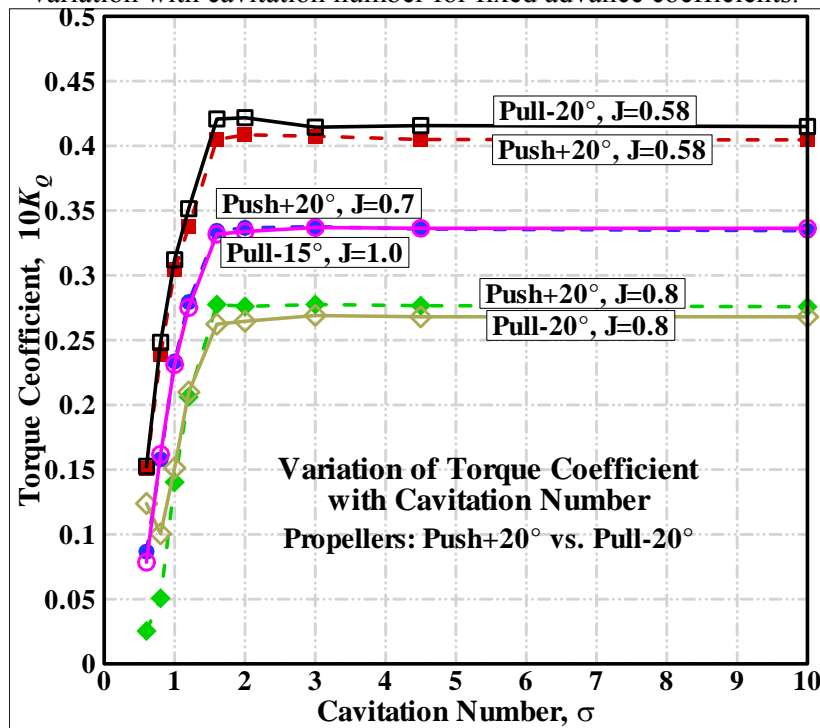


Figure 4-24. Comparison of torque coefficients (Push+20° and Pull-20°) at different cavitation numbers for fixed advance coefficients.

4-5. Cavitation and Pattern Observations

The analysis of the propeller performance under cavitating conditions is best done on a case-by-case basis, and a general trend in the performance is obtained. The current testing was carried out for a wide range of advance coefficients (from lowest possible and the highest allowed by tunnel limitations), at a total of nine cavitation numbers. These cavitation numbers were held constant for each individual set of J values. The cavitation observations were made under stroboscopic lighting for all the conditions mentioned in table 2. Video recordings were also taken using a MiniDV digital video camera capturing at 30 frames per second. The footage obtained for all the trials was taken from the suction side of the propeller. This is not fully in accordance with ITTC standards (ITTC – Recommended Procedures 2002), which require footage to be taken from both the pressure side and suction side to give fullest possible picture of the cavitation patterns. However, the cavitation pattern occurred on the suction side has the most practical value and is always the prime concern to the designer. Cavitation on the pressure side often occurs at high advance coefficients while producing negative thrust and carries little practical significance. Detailed sketches of the cavitation patterns were drawn for all the test conditions for both the pressure side and the suction side. Three radial lines (at $0.05R$, $0.07R$, $0.09R$) and one midchord line were drawn on each side of all blades of all the propellers to facilitate locating the cavitation patterns.

The appearance of the cavitation patterns for all of the four propellers at all cavitation numbers tested are presented in snapshot picture format taken from the video footage. The test conditions together with the quantitative performance are presented with each picture. The patterns are self-explanatory and detailed discussion of all the patterns is out of the scope of the paper. The cavitation patterns varied from steady sheet cavitation on the whole surface of the blade suction side at the lowest tested cavitation number ($\sigma_n=0.6$), to steady/unsteady sheet cavitation with unsteady streak cavitation on a portion of the blade surface accompanied by thick tip vortex cavitation at moderate cavitation number ($\sigma_n=1.0\sim 2.0$), to thin tip vortex cavitation at atmospheric pressure at low J values. All four of the propellers show similar cavitation patterns at the same operating conditions.

The photographs in Figures A-1 to A-4 show examples of the development of cavitation. In each figure, each row represents snapshots of a propeller operating at a particular cavitation number and at each row, the columns show the propeller in operation at the particular cavitation number as the advance coefficient increases from left to right. For a given

cavitation number as the propeller advance coefficient increases (by increasing speed of advance, V_A for a fixed rps) the amount of cavitation on the blade surface tends to decrease. The tip vortex cavity thickness and amount of sheet cavitation over the blade surface decreased as the speed of advance increased (inflow angle of attack decreased).

As shown in figure A-1, as one looks down vertically along the first column of the figure, the amount of steady sheet cavitation increased and the thickness of tip vortex cavity increased, which results in performance deterioration. But as one goes along each row, as the advance coefficient increased, the amount of surface cavitation decreased. For high J , it was very difficult to notice the cavitation patterns because of the interference of bubbles (may be because of high oxygen contents and possible cavitation of tunnel impeller). At the lowest cavitation number ($\sigma_n=0.6$) for this propeller the entire suction side of the blades was cavitating (steady sheet cavitation) throughout all advance coefficients. As the cavitation number increased the amount of sheet cavitation decreased and some steady/unsteady streak cavitation appeared with improvement of performance. At the design cavitation number ($\sigma_n=3.0$) only thick tip vortex cavitation was observed with occasional occurrence of steady/unsteady sheet cavitation at the suction side around the leading edge. As the cavitation number increased further, the sheet cavitation disappeared completely and the thickness of tip cavitation decreased with almost no change in performance. There was hardly any cavitation at the pressure side of the blades except at very high advance coefficients ($J>0.9$). For most of the cavitation numbers at this high J , the propeller produced negative thrust, which was of little practical interest.

The other three propellers gave similar and consistent cavitation patterns (see Figure A-2 (Push+20), A-3 (Push-15) and A-4 (Push-20)). It should be noted here that the four propellers have the same design blade sections and only differ at hub taper angle. The blade section near the hub changes because of the solid body interaction of blade and the hub. This change is responsible for the change of flow pattern around the blade root and hence the local cavitation characteristics. The cavitation types that most influence the performance are tip vortex and sheet. The patterns of these two types are similar for the propellers.

4-6. Effect of Taper Angle on Cavitation Inception:

Cavitation inception testing was conducted in the tunnel with the propellers mounted on the upstream shaft and in the open jet test section. The brass-constructed propellers were radially marked in black at three radial positions to facilitate cavitation inception visualization. Throughout the cavitation inception testing, the propeller revolution was set to two different numbers (20 rps and 15 rps).

Inception points at each advance condition were established by setting constant water speed and propeller revolutions and then decreasing tunnel pressure until cavitation developed. Once the tunnel pressure at cavitation inception point was noted, the pressure was lowered further to get a steady cavitation pattern. Then the tunnel pressure was raised again to the point when the cavitation just disappeared (cavitation desinence). Static pressure values entering into the calculation of cavitation number at the point of cavitation inception are those pressures at the propeller shaft line. During the runs, air content was varied between 20 and 35% saturation at atmospheric pressure. The water temperature varied between 18°C to 20°C. The cavitation inception curves for all four propellers (see Figures 4-25 and 4-26) show that for low advance coefficients the cavitation inception occurs at high tunnel pressure, but as the advance coefficient increases, the inception occurs at comparatively low tunnel pressure. As the advance coefficient increases further, the tunnel pressure at which inception occurred increased. It should be noted here that for the first two advance coefficients tested, the inception occurs at the suction side (tip cavitation) of the propeller blade, but for the two higher advance coefficients, inception occurs at the pressure side (sheet cavitation), which means the propellers were operating at negative hydrodynamic angles of attack. The cavitation desinence curves show a similar trends but it occurs at a little bit higher tunnel pressure.

The effects of hub taper angle on cavitation inception and desinence are shown in Figures 4-25(a) and 4-26(a). From these figures it can be seen that hub taper angle does not have significant effect on the visual cavitation inception and desinence for moderate advance coefficients. Inclusion of hub taper angle changes the blade sections around the blade roots, but cavitation inception mainly occurs around the blade tip (tip vortex cavitation) unless the blade is very thick (then usually bubble or cloud cavitation occurs at the midchord position where the blade section is mostly thick).

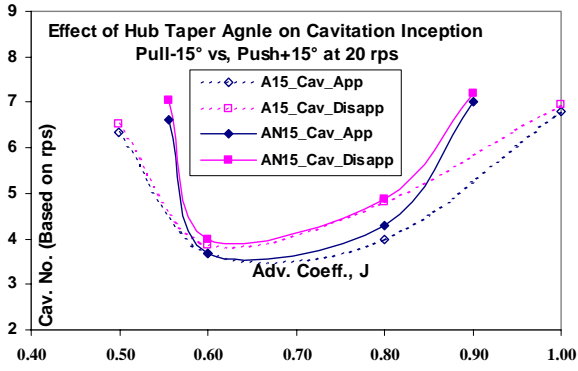


Figure 4-25 (a): Comparison of cavitation inception and desinence curves at different J_s for the Push +15° and the Pull-15° operating at 20 rps.

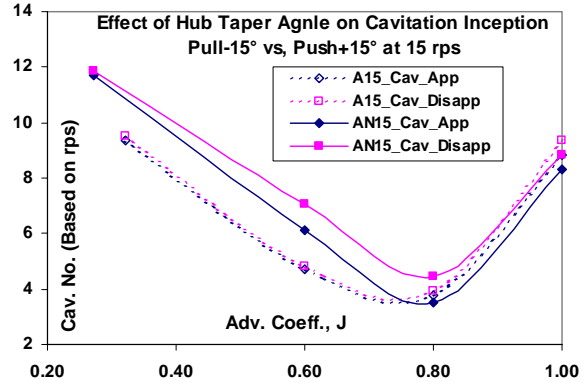


Figure 4-26 (b): Comparison of cavitation inception and desinence curves at different J_s for the Push +15° and the Pull-15° operating at 15 rps.

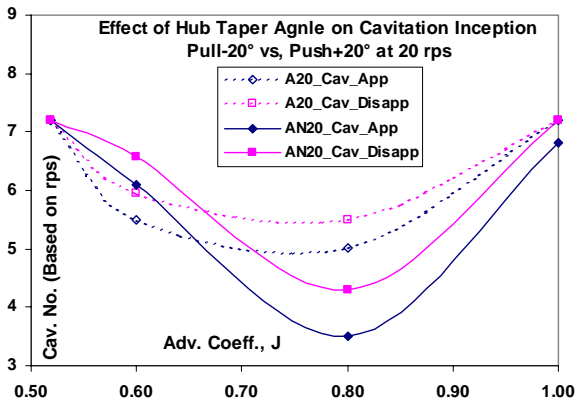


Figure 4-26 (a): Comparison of cavitation inception and desinence curves at different J_s for the Push +20° and the Pull-20° operating at 20 rps.

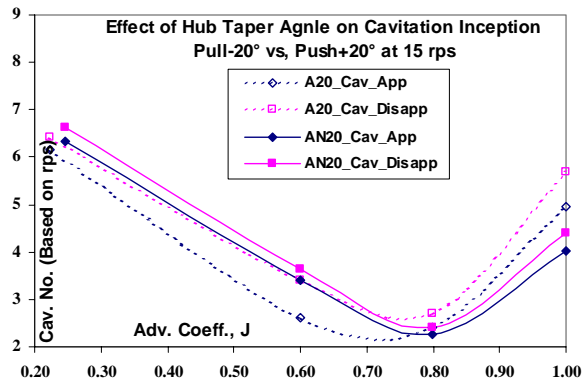


Figure 4-26 (b): Comparison of cavitation inception and desinence curves at different J_s for the Push +20° and the Pull-20° operating at 15 rps.

Chapter 5. Concluding Remarks

This research work aimed to compare the propulsive performance of a puller and pusher propeller at different cavitation conditions. The cavitation tunnel tests, which were carried out at the cavitation tunnel of the Institute for Ocean technology (IOT), National Research Council (NRC) Canada, involved the measurements of propulsive performance of four propellers with different hub taper angles under several cavitating conditions. Observation of the cavitation characteristics and visual cavitation inception tests were also performed. The cavitation inception tests were conducted with a view to examine the effects of hub taper angle on cavitation inception. Additional tests were done at the design cavitation number with three different propeller rotational speeds to investigate the *Reynolds Number* effects at design conditions. The following conclusions were reached from the analyses of the data acquired.

For each of the four propellers, the values of K_T and K_Q tend to increase as the cavitation number, σ_n , is increased from 0.6 to 1.6. As the cavitation number increased further, the values of K_T and K_Q decreased before it started to stabilize at the design cavitation number of ($\sigma_{design}=3.0$). It is also clear from the video footage that the amount of cavitation on blade surface increased as the cavitation number decreased. All of the four propellers showed similar cavitation pattern at the same operating conditions.

The study of the *Reynolds Number* effect revealed that the measured performance for all of the four propellers at the design cavitation number ($\sigma_{design}=3.0$) at 20 rps were almost the same as that of the 25 rps, while very narrow gaps lay between that of 20 rps and 15 rps. This indicated that *Reynolds Number* effects were very limited for the model propellers with sufficiently large diameter and could be neglected when the propeller operation speed exceeded 15 rps.

Increasing the hub taper angle increased the torque, and this effect increased with advance coefficient. For thrust, increasing the taper angle also increased the thrust but not with the same magnitude as torque coefficient and the increase is more obvious at higher advance coefficient. The net effect on the propeller efficiency was that the efficiency decreased for larger hub angles and the effect was more pronounced for higher advance coefficient. The similar effects were observed for all the cavitation conditions except at low cavitation number (cavitation number less than 1.0) where the comparison was not very obvious.

It was observed that the push configuration propellers consistently had lower torque and

thrust coefficients than their puller counterparts tested under the same cavitation conditions. The increase in thrust and torque for the puller propellers as compared to those of the pusher ones were more obvious at lower advance coefficient values. The overall effect on the propeller efficiency is a slight decrease of efficiency for the pusher propellers, particularly for the lightly loaded conditions.

The difference in propulsive performance coefficient values between the Push+15 and Pull-15 propellers remained the same at all cavitation numbers for the entire range of advance coefficients. The difference is almost equal to the difference that exists in open water condition. This means the relative performance of the pushing and the pulling propellers are almost same under cavitation. For the puller propeller with -20° taper angle the performance was not necessarily better than or equal to the pusher propeller with $+20^\circ$ taper angle. In this case, for most of the cavitation numbers the performance curves of the two propellers overlap, which means that the propeller performance is almost independent of the taper angle when the angle is too high ($\geq \pm 20^\circ$).

Visual inspection of the cavitation inception and desinence (tip vortex and sheet cavitation type) of the four propellers revealed that hub taper angle does not have significant effect on the visual cavitation inception and desinence for moderate advance coefficients.

The previous study performed by the authors revealed that the puller propeller performs better than a pusher propeller in open water conditions. The present study was aimed to see how the performance varies under cavitating condition. The study revealed that the puller propeller with moderate hub taper angle performs equally to the pusher ones for all cavitation conditions tested. The reason for the difference in performance between a pushing propeller and a pulling propeller is attributed to the poor sectional pressure distributions at the blade root sections of a pushing propeller (same as in the open water conditions). This study opens the scope of designing a pusher propeller by optimizing the abnormal blade sections, which will perform better than or equivalent to the corresponding puller propeller with the additional advantage of reduced fluctuation forces on the strut.

Acknowledgements

The authors would like to express their gratitude to the Natural Sciences and Engineering Research Council (NSERC), the National Research Council (NRC), Memorial University, Oceanic Consulting Corp., and Thordon Bearings Inc. for their financial and other support. Thanks are also extended to the staff at the NRC Institute for Ocean Technology for their

assistance. The authors would like to extend special thanks to Mr. Darrell Sparks for his help in the experimental set-up.

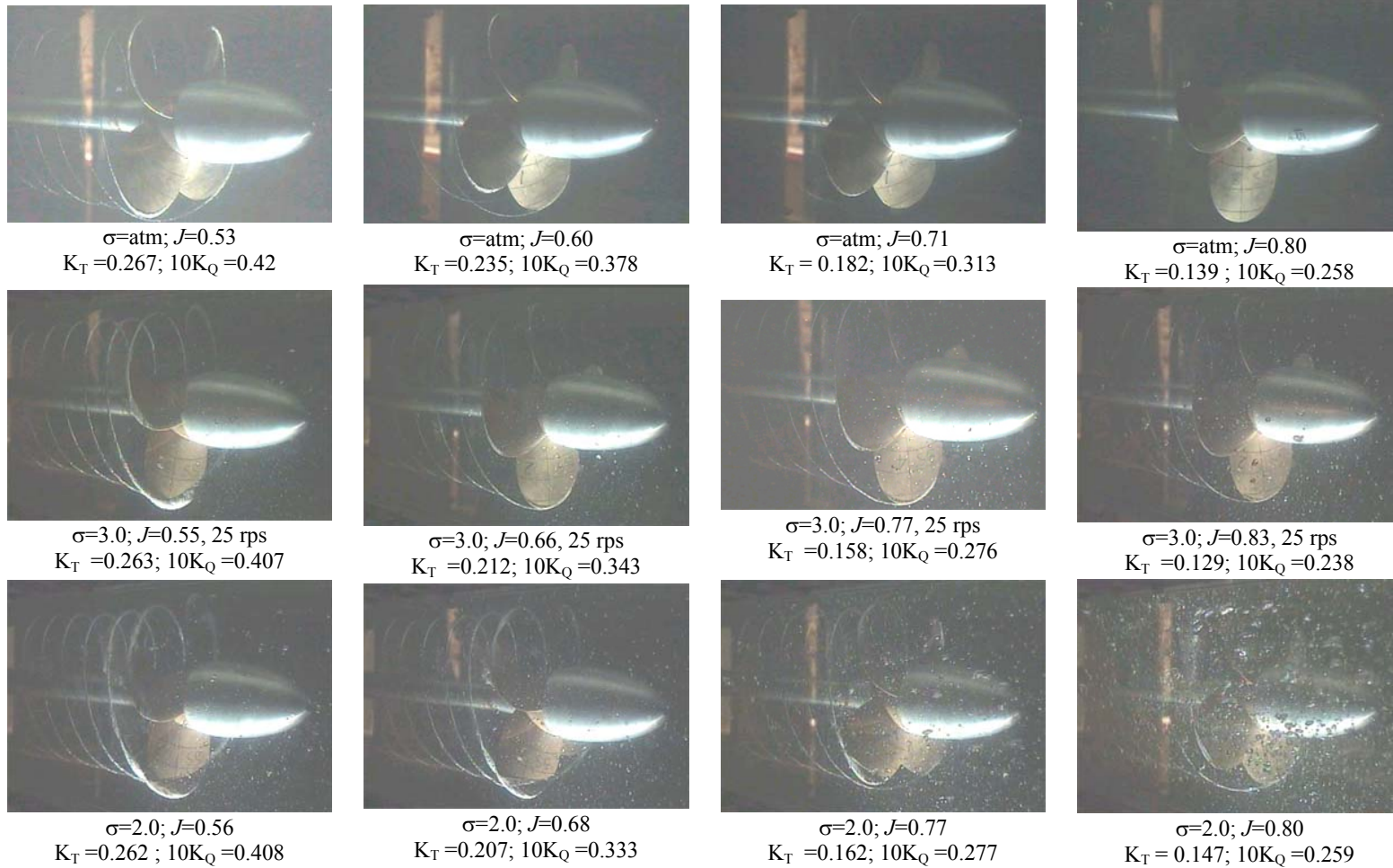
References

- ATLAR, M, TAKINACI, A.C., KORKUT, E., SASAKI N. & AONO, T. 2001 Cavitation Tunnel Tests for Propeller Noise of a FRV and Comparisons with Full-Scale Measurements. CAV2001: Session B8.007, pp.
- BRENT, K. 2004 Performance testing of a podded propeller in the cavitation tunnel. Report No. LM-2004-12, IOT, NRC Canada.
- DENNY, S. B. 1968 Cavitation and Open Water Performance tests of a series of propellers designed by lifting surface methods. Report 2878, Dept of Navy, naval ship research and development center, Washington, D. C. 20007.
- DOUCET, M. J. 1992 Cavitation tunnel instruction manual. Report No. OERC92-TR-HYD-92005, Ocean Engineering Research Centre, Faculty of Engineering and Applied Science, Memorial University of Newfoundland, St. John's, NL.
- FRIESCH, J. 2004 Cavitation and vibration investigations for podded drives. In Proc. of the 1st International Conference on Technological Advances in Podded Propulsion, 13p.
- GAWN, R.W.L. & BURRIL, L.C. 1957 Effect of cavitation on the performance of a series of 16 in model propellers. Transactions INA, Vol. 99, pp. 690-728.
- ISLAM, M. F., TAYLOR, R., QUINTON J., VEITCH, B., BOSE, N., COLBOURNE, B. & LIU, P. 2004 Numerical investigation of propulsive characteristics of podded propeller. In Proc. of the 1st International Conference on Technological Advances in Podded Propulsion, pp. 513-525.
- ISLAM, M. F. 2004 Numerical investigation on effects of hub taper angle and Pod-strut geometry on propulsive performance of pusher Propeller configurations. Master's thesis, Memorial University of Newfoundland.
- ITTC – Recommended Procedures, (2002), “Testing and Extrapolation Methods: Propulsion, Cavitation Model – Scale Cavitation Test”, 7.5-02-03-03.1, 9p.
- JESSUP, S., BOSE, N., DUGUÉ, C., ESPOSITO, P.G., HOLTROP, J., LEE, J.T., MEWIS, F., PUSTOSHNY, A., SALVATORE, F., SHIROSE, Y., (2002). The Propulsion Committee: Final Report and Recommendations to the 23rd ITTC, Proceedings of the 23rd ITTC - Volume I, pp. 89-151.
- LINDGREN H. (1963), “Propeller cavitation experiments in uniform flow: A note on test procedure, corrections and presentation”, 10th ITTC Cavitation Committee Reports: Appendix I, pp 114-123.

- LIU, P., BOSE, N., & COLBOURNE, B. 2001 Incorporation of a Critical Pressure Scheme into a Time Domain Panel Method for Propeller Sheet Cavitation. International Workshop on Ship Hydrodynamics (IWSH), Wuhan, China. pp.
- LIU, P. (2006) "The Design of a Podded Propeller Base Model Geometry and Prediction of Its hydrodynamics", Technical Report no. TR-2006-16, Institute for Ocean Technology, National Research Council Canada, 16 p.
- MATSUBA, N., KUROBE, Y., UKON, Y., KUDO, T. & OKAMOTO, M. 1994 Experimental investigation into the performance of super-cavitating propellers. Papers of ship research institute, 31(5), pp. 192-251
- PEREIRA, F., SALVATORE, F., FELICE, F.D. & ELEFANTE, M. 2002 Experimental and Numerical Investigation of the Cavitation Pattern on a Marine Propeller. 24th Symposium on Naval Hydrodynamics, Fukuoka, Japan, 8-13 July, pp.
- PEREIRA, F., SALVATORE, F., FELICE F. D. & SOAVE, M. 2004 Experimental Investigation of a Cavitating Propellers in Non-Uniform Inflow. ONR 2004, pp.
- PUSTOSHNY, A. V., & KAPRANTSEV, S. V. 2001 Azipod Propeller Blade Cavitation Observation During Ship Manoeuvring. Forth International Symposium on Cavitation (CAV2001), June 20-23, pp.
- TAYLOR, R. S. (2006), "Experimental Investigation of the Influence of Hub Taper Angle on the Performance of Push and Pull Configuration Podded Propellers", Master in Engineering, Memorial University of Newfoundland, Canada, 150p.
- WALKER, D. L. N. 1996 The influence of blockage and cavitation on the hydrodynamic performance of ice class propellers in blocked flow. PhD. Thesis, Memorial University of Newfoundland.
- WALKER, D. L. N. 1995 The effects of propeller blade root fillet design on cavitation performance. CR-1995-04, Marineering Limited, IMD, NRC.

Appendix A

Figure A-1. Photographs showing back cavitation for 15° Pusher Propeller at different cavitating conditions.





$\sigma=1.6; J=0.53$
 $K_T = 0.262; 10K_Q = 0.42$



$\sigma=1.6; J=0.60$
 $K_T = 0.239; 10K_Q = 0.384$



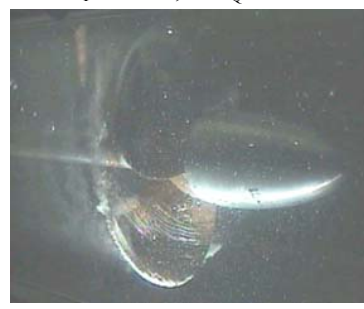
$\sigma=1.6; J=0.65$
 $K_T = 0.218; 10K_Q = 0.354$



$\sigma=1.6; J=0.77$
 $K_T = 0.163; 10K_Q = 0.28$



$\sigma=1.0; J=0.43$
 $K_T = 0.221; 10K_Q = 0.379$



$\sigma=1.0; J=0.50$
 $K_T = 0.201; 10K_Q = 0.348$



$\sigma=1.0; J=0.60$
 $K_T = 0.17; 10K_Q = 0.293$



$\sigma=1.0; J=0.81$
 $K_T = 0.057; 10K_Q = 0.132$



$\sigma=0.6; J=0.37$
 $K_T = 0.171; 10K_Q = 0.295$



$\sigma=0.6; J=0.51$
 $K_T = 0.114; 10K_Q = 0.207$

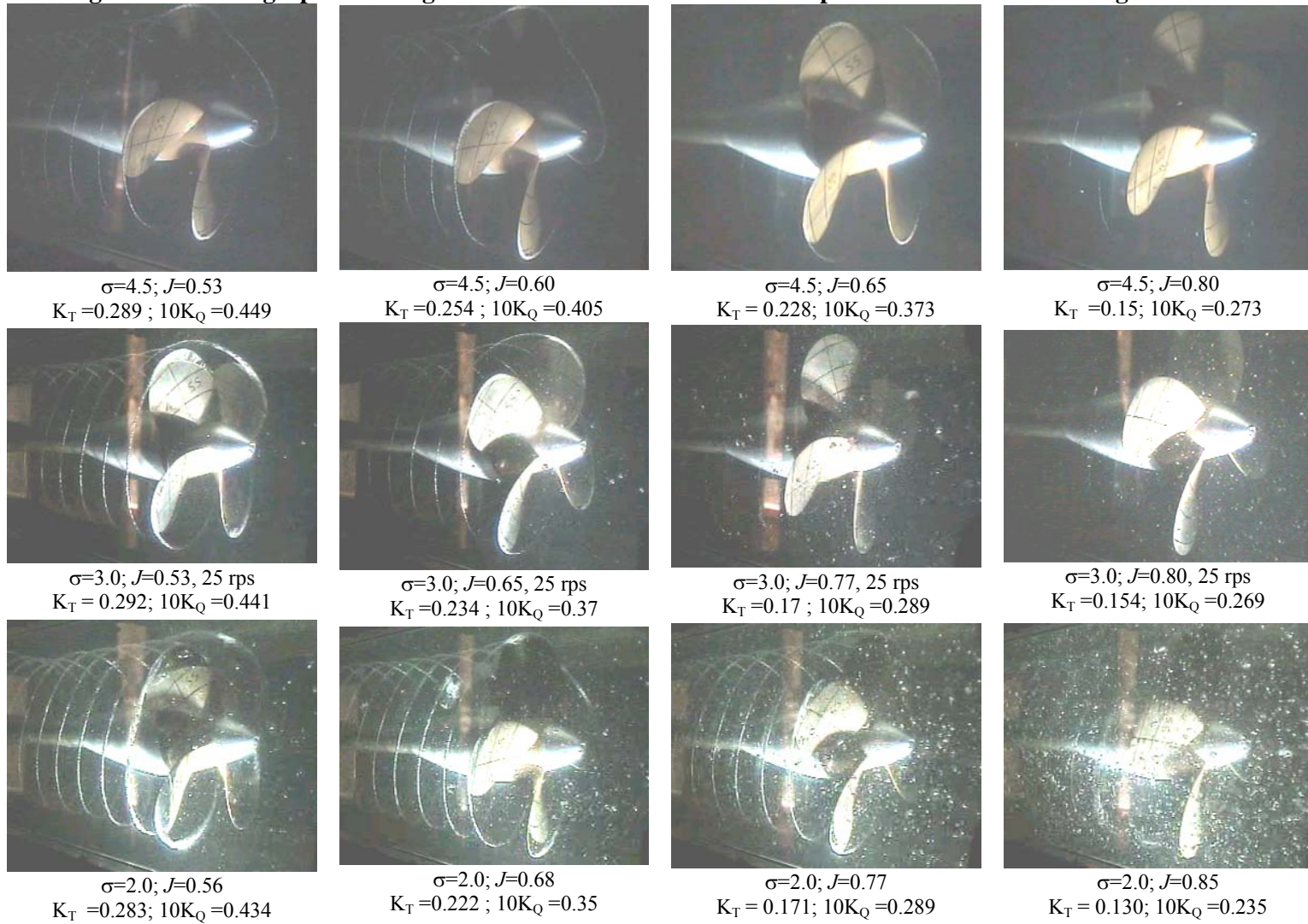


$\sigma=0.6; J=0.68$
 $K_T = 0.045; 10K_Q = 0.102$



$\sigma=0.6; J=0.74$
 $K_T = 0.0256; 10K_Q = 0.074$

Figure A-2. Photographs showing back cavitation for -15° Puller Propeller at different cavitating conditions.





$\sigma=1.6; J=0.55$
 $K_T=0.268; 10K_Q=0.426$



$\sigma=1.6; J=0.65$
 $K_T=0.237; 10K_Q=0.38$



$\sigma=1.6; J=0.71$
 $K_T=0.205; 10K_Q=0.334$



$\sigma=1.6; J=0.74$
 $K_T=0.188; 10K_Q=0.311$



$\sigma=1.0; J=0.47$
 $K_T=0.232; 10K_Q=0.376$



$\sigma=1.0; J=0.60$
 $K_T=0.191; 10K_Q=0.314$



$\sigma=1.0; J=0.68$
 $K_T=0.151; 10K_Q=0.257$



$\sigma=1.0; J=0.74$
 $K_T=0.117; 10K_Q=0.211$



$\sigma=0.6; J=0.4$
 $K_T=0.168; 10K_Q=0.28$



$\sigma=0.6; J=0.5$
 $K_T=0.133; 10K_Q=0.225$

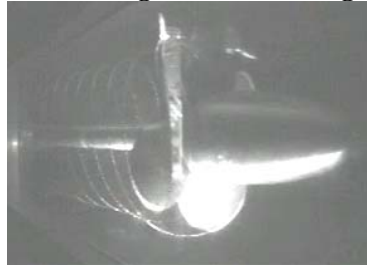


$\sigma=0.6; J=0.6$
 $K_T=0.093; 10K_Q=0.166$



$\sigma=0.6; J=0.68$
 $K_T=0.056; 10K_Q=0.106$

Figure A-3. Photographs showing back cavitation for 20° Pusher Propeller at different cavitating conditions.



$\sigma = \text{atm}; J = 0.53$
 $K_T = 0.271; 10K_Q = 0.434$



$\sigma = \text{atm}; J = 0.59$
 $K_T = 0.242; 10K_Q = 0.398$



$\sigma = \text{atm}; J = 0.71$
 $K_T = 0.185; 10K_Q = 0.328$



$\sigma = \text{atm}; J = 0.83$
 $K_T = 0.130; 10K_Q = 0.257$



$\sigma = 3.0; J = 0.54, 25 \text{ rps}$
 $K_T = 0.27; 10K_Q = 0.43$



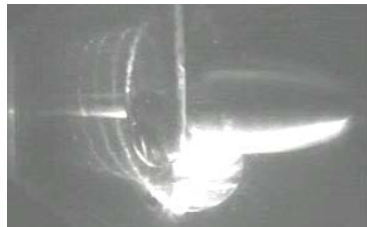
$\sigma = 3.0; J = 0.62, 25 \text{ rps}$
 $K_T = 0.234; 10K_Q = 0.384$



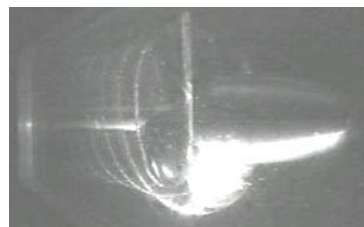
$\sigma = 3.0; J = 0.68, 25 \text{ rps}$
 $K_T = 0.205; 10K_Q = 0.349$



$\sigma = 3.0; J = 0.80, 25 \text{ rps}$
 $K_T = 0.148; 10K_Q = 0.277$



$\sigma = 1.6; J = 0.56$
 $K_T = 0.251; 10K_Q = 0.414$



$\sigma = 1.6; J = 0.65$
 $K_T = 0.216; 10K_Q = 0.364$



$\sigma = 1.6; J = 0.71$
 $K_T = 0.190; 10K_Q = 0.329$



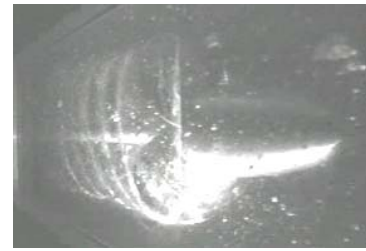
$\sigma = 1.6; J = 0.82$
 $K_T = 0.14; 10K_Q = 0.264$



$\sigma=1.2; J=0.56$
 $K_T = 0.192; 10K_Q = 0.332$



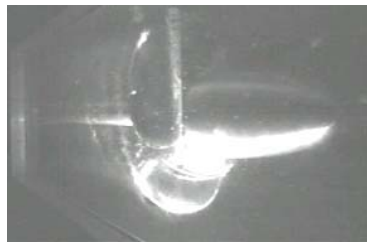
$\sigma=1.2; J=0.62$
 $K_T = 0.17; 10K_Q = 0.304$



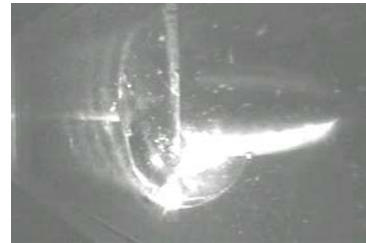
$\sigma=1.2; J=0.68$
 $K_T = 0.142; 10K_Q = 0.266$



$\sigma=1.2; J=0.77$
 $K_T = 0.091; 10K_Q = 0.195$



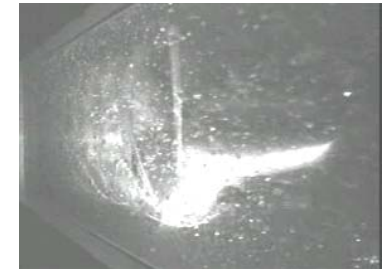
$\sigma=1.0; J=0.56$
 $K_T = ; 10K_Q =$



$\sigma=1.0; J=0.62$
 $K_T = ; 10K_Q =$



$\sigma=1.0; J=0.68$
 $K_T = ; 10K_Q =$



$\sigma=1.0; J=0.74$
 $K_T = ; 10K_Q =$



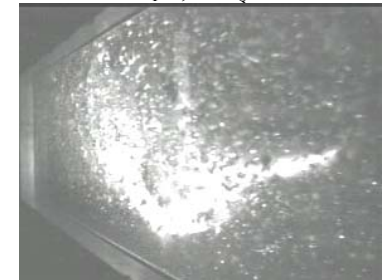
$\sigma=0.6; J=0.56$
 $K_T = 0.123; 10K_Q = 0.321$



$\sigma=0.6; J=0.62$
 $K_T = 0.094; 10K_Q = 0.188$

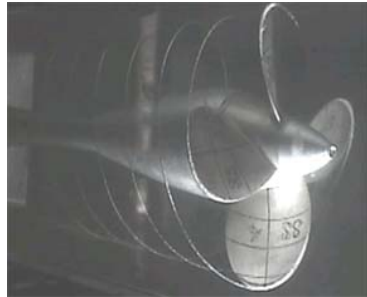


$\sigma=0.6; J=0.68$
 $K_T = 0.07; 10K_Q = 0.153$



$\sigma=0.6; J=0.74$
 $K_T = 0.043; 10K_Q = 0.11$

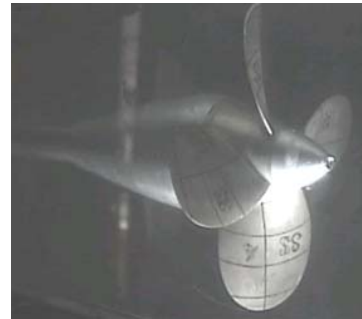
Figure A-4. Photographs showing back cavitation for -20° Puller Propeller at different cavitating conditions.



$\sigma = \text{atm}; J = 0.53$
 $K_T = 0.279; 10K_Q = 0.445$



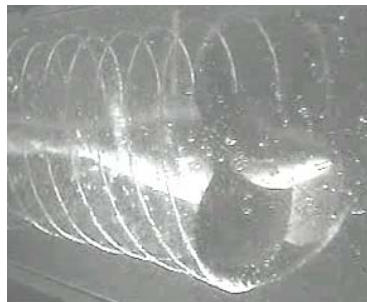
$\sigma = \text{atm}; J = 0.60$
 $K_T = 0.243; 10K_Q = 0.402$



$\sigma = \text{atm}; J = 0.68$
 $K_T = 0.2; 10K_Q = 0.35$



$\sigma = \text{atm}; J = 0.80$
 $K_T = 0.135; 10K_Q = 0.268$



$\sigma = 3.0; J = 0.51, 25 \text{ rps}$
 $K_T = 0.274; 10K_Q = 0.455$



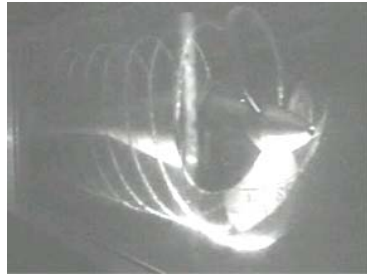
$\sigma = 3.0; J = 0.59, 25 \text{ rps}$
 $K_T = 0.254; 10K_Q = 0.412$



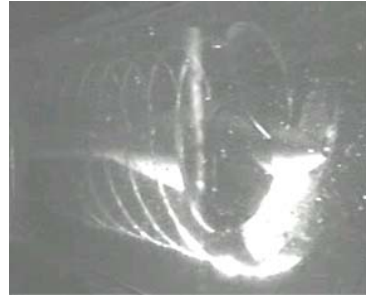
$\sigma = 3.0; J = 0.65, 25 \text{ rps}$
 $K_T = 0.226; 10K_Q = 0.373$



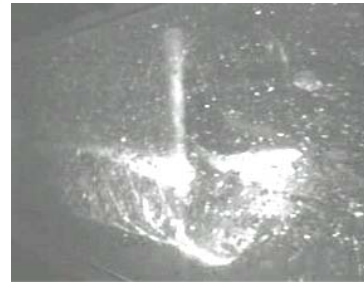
$\sigma = 3.0; J = 0.71, 25 \text{ rps}$
 $K_T = 0.192; 10K_Q = 0.331$



$\sigma=2.0; J=0.56$
 $K_T=0.275; 10K_Q=0.436$



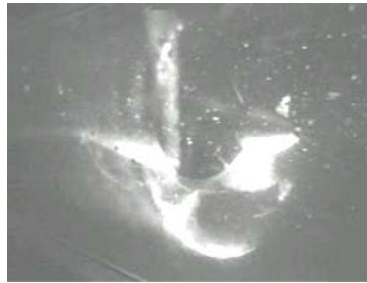
$\sigma=2.0; J=0.62$
 $K_T=0.242; 10K_Q=0.392$



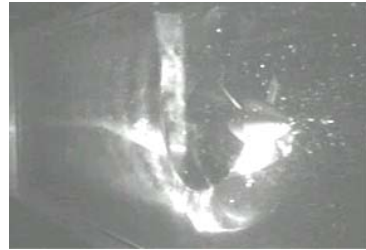
$\sigma=2.0; J=0.74$
 $K_T=0.174; 10K_Q=0.305$



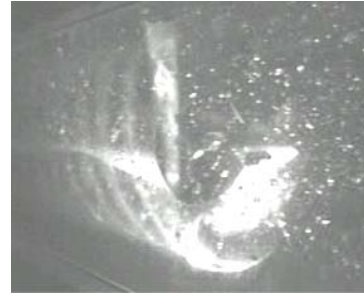
$\sigma=2.0; J=0.83$
 $K_T=0.125; 10K_Q=0.244$



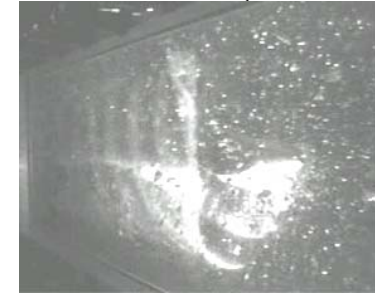
$\sigma=1.0; J=0.44$
 $K_T=0.232; 10K_Q=0.388$



$\sigma=1.0; J=0.56$
 $K_T=0.185; 10K_Q=0.323$



$\sigma=1.0; J=0.62$
 $K_T=0.162; 10K_Q=0.187$



$\sigma=1.0; J=0.71$
 $K_T=0.12; 10K_Q=0.223$



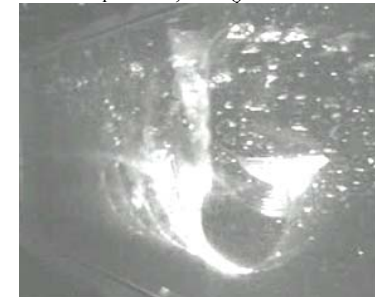
$\sigma=0.6; J=0.23$
 $K_T=0.207; 10K_Q=0.352$



$\sigma=0.6; J=0.35$
 $K_T=0.17; 10K_Q=0.292$



$\sigma=0.6; J=0.47$
 $K_T=0.132; 10K_Q=0.234$



$\sigma=0.6; J=0.56$
 $K_T=0.088; 10K_Q=0.169$

Appendix B

Table B-1. Experimental data of the four propellers at different cavitating conditions.

Push+15°				Pull-15°				Push+20°				Pull-20°			
At Atmospheric Pressure Condition															
J	KT	10KQ	Eta	J	KT	10KQ	Eta	J	KT	10KQ	Eta	J	KT	10KQ	Eta
0.53	0.2684	0.4251	0.5319	0.38	0.2970	0.4597	0.3911	0.34	0.3175	0.4934	0.3510	0.53	0.2577	0.4189	0.5198
0.56	0.2523	0.4052	0.5579	0.52	0.2541	0.4033	0.5191	0.37	0.3027	0.4768	0.3724	0.61	0.2176	0.3709	0.5715
0.61	0.2318	0.3803	0.5879	0.58	0.2261	0.3683	0.5703	0.48	0.2482	0.4119	0.4594	0.65	0.1993	0.3482	0.5911
0.64	0.2144	0.3582	0.6107	0.62	0.2100	0.3484	0.5915	0.59	0.2024	0.3563	0.5373	0.68	0.1828	0.3276	0.6056
0.68	0.1984	0.3373	0.6318	0.65	0.1946	0.3294	0.6125	0.71	0.1627	0.3081	0.5949	0.72	0.1650	0.3056	0.6159
0.71	0.1824	0.3175	0.6467	0.68	0.1805	0.3117	0.6307	0.82	0.1206	0.2494	0.6304	0.75	0.1486	0.2850	0.6230
0.77	0.1510	0.2772	0.6704	0.72	0.1659	0.2941	0.6438	0.93	0.0735	0.1834	0.5935	0.78	0.1321	0.2645	0.6225
0.81	0.1341	0.2550	0.6764	0.75	0.1517	0.2758	0.6567	1.05	0.0179	0.1063	0.2801	0.82	0.1145	0.2415	0.6178
0.84	0.1185	0.2341	0.6766	0.78	0.1363	0.2552	0.6665	1.15	-0.0432	0.0180	-4.4264	0.85	0.0982	0.2200	0.6049
0.87	0.1017	0.2104	0.6726	0.82	0.1216	0.2352	0.6725					0.89	0.0812	0.1973	0.5800
0.9	0.0870	0.1896	0.6607	0.85	0.1080	0.2151	0.6797					0.92	0.0651	0.1749	0.5441
0.94	0.0687	0.1648	0.6236	0.91	0.0790	0.1744	0.6598					0.95	0.0488	0.1514	0.4882
0.97	0.0518	0.1419	0.5641	0.99	0.0452	0.1271	0.5578					0.99	0.0324	0.1270	0.4000
1.01	0.0314	0.1138	0.4424	1.05	0.0100	0.0775	0.2154					1.02	0.0158	0.1020	0.2511
1.04	0.0120	0.0862	0.2310	1.12	-0.0297	0.0204	-2.5931					1.05	-0.0029	0.0738	-0.0653
1.11	-0.0296	0.0253	-2.0592									1.12	-0.0433	0.0143	-5.4022
At Cavitation Number=0.65															
J	KT	10KQ	Eta	J	KT	10KQ	Eta	J	KT	10KQ	Eta	J	KT	10KQ	Eta
0.37	0.1235	0.2029	0.3198	0.36	0.1612	0.2806	0.3270	0.54	0.0869	0.1715	0.4378	0.37	0.1235	0.2029	0.3198
0.44	0.1473	0.2518	0.4079	0.4	0.1491	0.2614	0.3667	0.57	0.0706	0.1455	0.4389	0.44	0.1473	0.2518	0.4079
0.5	0.1189	0.2076	0.4529	0.43	0.1397	0.2467	0.3910	0.61	0.0514	0.1154	0.4338	0.5	0.1189	0.2076	0.4529
0.53	0.1130	0.1994	0.4743	0.47	0.1216	0.2176	0.4165	0.64	0.0506	0.1149	0.4489	0.53	0.1130	0.1994	0.4743
0.56	0.1061	0.1890	0.5023	0.5	0.1041	0.1902	0.4373	0.67	0.0370	0.0944	0.4196	0.56	0.1061	0.1890	0.5023
0.6	0.0913	0.1674	0.5170	0.54	0.0857	0.1623	0.4526	0.69	0.0298	0.0828	0.3977	0.6	0.0913	0.1674	0.5170
0.66	0.0493	0.1054	0.4953	0.57	0.0781	0.1505	0.4705	0.73	0.0225	0.0731	0.3581	0.66	0.0493	0.1054	0.4953
0.69	0.0405	0.0926	0.4831	0.6	0.0742	0.1445	0.4923	0.77	0.0133	0.0601	0.2697	0.69	0.0405	0.0926	0.4831
0.72	0.0355	0.0856	0.4786	0.64	0.0633	0.1282	0.4996					0.72	0.0355	0.0856	0.4786
				0.7	0.0296	0.0793	0.4193								
At Cavitation Number=0.86															
J	KT	10KQ	Eta	J	KT	10KQ	Eta	J	KT	10KQ	Eta	J	KT	10KQ	Eta
0.39	0.2023	0.3383	0.3710	0.35	0.1888	0.3234	0.3241	0.56	0.1226	0.2304	0.4766	0.4	0.1909	0.3308	0.3666
0.55	0.1534	0.2625	0.5150	0.4	0.1782	0.3063	0.3707	0.6	0.1094	0.2107	0.4941	0.43	0.1852	0.3224	0.3927
0.59	0.1438	0.2483	0.5411	0.43	0.1722	0.2967	0.3977	0.63	0.0941	0.1879	0.5033	0.46	0.1751	0.3067	0.4198
0.62	0.1312	0.2302	0.5634	0.46	0.1633	0.2830	0.4254	0.67	0.0790	0.1654	0.5057	0.49	0.1642	0.2897	0.4451
0.65	0.1158	0.2076	0.5793	0.5	0.1534	0.2687	0.4524	0.7	0.0691	0.1512	0.5087	0.53	0.1510	0.2695	0.4715
0.69	0.0931	0.1749	0.5830	0.53	0.1465	0.2585	0.4775	0.73	0.0590	0.1353	0.5087	0.56	0.1334	0.2401	0.4958
0.72	0.0764	0.1504	0.5838	0.56	0.1388	0.2467	0.5027	0.77	0.0387	0.1018	0.4635	0.6	0.1173	0.2165	0.5129
0.76	0.0670	0.1366	0.5908	0.6	0.1302	0.2342	0.5267	0.8	0.0035	0.0430	0.1039	0.63	0.0997	0.1908	0.5236
0.79	0.0435	0.1027	0.5315	0.63	0.1197	0.2191	0.5465					0.67	0.0842	0.1686	0.5301
0.82	0.0149	0.0578	0.3364	0.66	0.1057	0.1987	0.5600					0.7	0.0740	0.1537	0.5345
0.85	0.0064	0.0447	0.1938	0.69	0.0854	0.1694	0.5571					0.73	0.0644	0.1392	0.5389
				0.73	0.0580	0.1285	0.5244					0.76	0.0529	0.1221	0.5260
				0.77	0.0364	0.0945	0.4733					0.78	0.0401	0.1032	0.4850
				0.8	0.0222	0.0715	0.3966					0.8	0.0299	0.0883	0.4302
				0.82	0.0017	0.0373	0.0599					0.82	0.0197	0.0745	0.3467
At Cavitation Number=1.07															
J	KT	10KQ	Eta	J	KT	10KQ	Eta	J	KT	10KQ	Eta	J	KT	10KQ	Eta
0.45	0.2298	0.3774	0.4315	0.43	0.2100	0.3536	0.4023	0.56	0.1661	0.2981	0.4949	0.43	0.2179	0.3701	0.4061
0.58	0.1810	0.3041	0.5530	0.46	0.2013	0.3393	0.4363	0.59	0.1547	0.2815	0.5177	0.52	0.1863	0.3239	0.4807
0.61	0.1689	0.2865	0.5768	0.49	0.1942	0.3284	0.4622	0.62	0.1424	0.2642	0.5349	0.56	0.1741	0.3061	0.5036
0.65	0.1571	0.2701	0.5994	0.52	0.1861	0.3156	0.4898	0.66	0.1287	0.2459	0.5476	0.59	0.1614	0.2863	0.5291
0.68	0.1409	0.2476	0.6166	0.56	0.1753	0.2996	0.5185	0.69	0.1123	0.2230	0.5540	0.62	0.1483	0.2664	0.5519
0.71	0.1195	0.2184	0.6221	0.59	0.1641	0.2839	0.5442	0.72	0.0923	0.1950	0.5462	0.66	0.1335	0.2440	0.5710
0.75	0.0966	0.1869	0.6167	0.62	0.1511	0.2660	0.5636	0.76	0.0714	0.1614	0.5340	0.69	0.1179	0.2202	0.5891
0.79	0.0767	0.1586	0.6049	0.66	0.1256	0.2307	0.5712	0.8	0.0439	0.1170	0.4757	0.72	0.1036	0.2012	0.5913

0.85	0.0462	0.1123	0.5580	0.69	0.1091	0.2081	0.5797	0.83	0.0249	0.0857	0.3840	0.76	0.0842	0.1761	0.5769
0.92	-0.0013	0.0370	-0.0496	0.73	0.0954	0.1892	0.5836	0.86	0.0065	0.0542	0.1640	0.79	0.0598	0.1437	0.5263
				0.76	0.0846	0.1736	0.5889					0.83	0.0379	0.1125	0.4431
				0.79	0.0711	0.1540	0.5832					0.86	0.0266	0.0951	0.3836
				0.83	0.0515	0.1231	0.5508					0.89	0.0174	0.0800	0.3088
				0.86	0.0124	0.0589	0.2881					0.93	-0.0046	0.0433	-0.1552
				0.89	-0.0031	0.0367	-0.1187					0.94	-0.0113	0.0322	-0.5284

At Cavitation Number=1.26

J	KT	10KQ	Eta	J	KT	10KQ	Eta	J	KT	10KQ	Eta	J	KT	10KQ	Eta
0.47	0.2436	0.3973	0.4594	0.46	0.2297	0.3786	0.4438	0.55	0.1947	0.3351	0.5110	0.45	0.2392	0.4003	0.4250
0.58	0.2079	0.3427	0.5610	0.44	0.2327	0.3837	0.4283	0.59	0.1842	0.3212	0.5366	0.52	0.2135	0.3620	0.4889
0.61	0.1941	0.3227	0.5853	0.52	0.2125	0.3527	0.5004	0.62	0.1729	0.3067	0.5568	0.55	0.2023	0.3452	0.5166
0.65	0.1771	0.2973	0.6122	0.55	0.2012	0.3355	0.5282	0.65	0.1614	0.2915	0.5754	0.59	0.1900	0.3268	0.5432
0.68	0.1664	0.2837	0.6329	0.59	0.1832	0.3075	0.5572	0.69	0.1478	0.2737	0.5900	0.65	0.1699	0.2953	0.5976
0.71	0.1523	0.2660	0.6482	0.62	0.1717	0.2897	0.5852	0.72	0.1306	0.2508	0.5972	0.69	0.1485	0.2641	0.6151
0.74	0.1377	0.2468	0.6606	0.69	0.1531	0.2685	0.6230	0.75	0.1125	0.2252	0.6000	0.72	0.1344	0.2465	0.6255
0.78	0.1175	0.2200	0.6621	0.75	0.1218	0.2303	0.6345	0.79	0.0922	0.1970	0.5875	0.75	0.1191	0.2276	0.6283
0.81	0.0969	0.1921	0.6523	0.82	0.0799	0.1691	0.6175	0.82	0.0711	0.1648	0.5646	0.82	0.0819	0.1811	0.5914
0.85	0.0717	0.1560	0.6192	0.9	0.0091	0.0553	0.2355	0.86	0.0410	0.1175	0.4770	0.86	0.0601	0.1523	0.5384
0.92	0.0012	0.0432	0.0398	0.96	-0.0102	0.0323	-0.4814	0.89	-0.0043	0.0441	-0.1394	0.89	0.0344	0.1148	0.4251
				1.01	-0.0062	0.0391	-0.2526	0.93	-0.0152	0.0338	-0.6656	0.93	0.0092	0.0733	0.1840
												0.96	-0.0187	0.0249	-1.1489
												0.99	-0.0235	0.0161	-2.3087
												1.01	-0.0253	0.0160	-2.5388

At Cavitation Number=1.65

J	KT	10KQ	Eta	J	KT	10KQ	Eta	J	KT	10KQ	Eta	J	KT	10KQ	Eta
0.52	0.2679	0.4269	0.5217	0.51	0.2556	0.4123	0.4998	0.49	0.2579	0.4245	0.4697	0.49	0.2723	0.4432	0.4762
0.64	0.2223	0.3593	0.6290	0.55	0.2410	0.3897	0.5436	0.58	0.2272	0.3790	0.5566	0.58	0.2369	0.3908	0.5603
0.67	0.2075	0.3381	0.6575	0.58	0.2312	0.3752	0.5709	0.62	0.2155	0.3633	0.5810	0.61	0.2221	0.3689	0.5891
0.71	0.1910	0.3155	0.6801	0.64	0.2065	0.3397	0.6233	0.65	0.2033	0.3467	0.6044	0.65	0.2063	0.3471	0.6137
0.74	0.1745	0.2936	0.6996	0.71	0.1759	0.2982	0.6711	0.68	0.1914	0.3304	0.6253	0.68	0.1868	0.3210	0.6317
0.77	0.1564	0.2704	0.7120	0.78	0.1444	0.2570	0.6977	0.72	0.1758	0.3094	0.6468	0.72	0.1712	0.2998	0.6505
0.84	0.1242	0.2298	0.7226	0.85	0.1131	0.2157	0.7082	0.75	0.1612	0.2896	0.6628	0.75	0.1559	0.2797	0.6643
0.91	0.0853	0.1755	0.7014	0.92	0.0637	0.1450	0.6434	0.78	0.1454	0.2698	0.6712	0.78	0.1387	0.2568	0.6734
0.98	0.0127	0.0630	0.3147	0.99	-0.0094	0.0355	-0.4171	0.82	0.1308	0.2515	0.6748	0.82	0.1227	0.2374	0.6715
								0.85	0.1121	0.2270	0.6669	0.85	0.1065	0.2174	0.6626
								0.88	0.0881	0.1925	0.6427	0.88	0.0887	0.1944	0.6420
								0.92	0.0518	0.1378	0.5508	0.92	0.0697	0.1691	0.6025
								0.95	0.0146	0.0795	0.2791	0.95	0.0460	0.1353	0.5153
								0.99	-0.0164	0.0348	-0.7405	0.99	0.0149	0.0879	0.2664
												1.02	-0.0212	0.0304	-1.1354
												1.06	-0.0412	0.0012	-56.3546

At Cavitation Number=2.07

J	KT	10KQ	Eta	J	KT	10KQ	Eta	J	KT	10KQ	Eta	J	KT	10KQ	Eta
0.54	0.2732	0.4218	0.5551	0.54	0.2547	0.3994	0.5433	0.53	0.2568	0.4107	0.5278	0.51	0.2789	0.4413	0.5112
0.64	0.2243	0.3557	0.6421	0.52	0.2614	0.4086	0.5307	0.52	0.2632	0.4201	0.5151	0.55	0.2587	0.4132	0.5450
0.67	0.2077	0.3348	0.6643	0.58	0.2359	0.3729	0.5872	0.58	0.2370	0.3841	0.5717	0.58	0.2428	0.3921	0.5732
0.71	0.1915	0.3144	0.6846	0.61	0.2208	0.3530	0.6120	0.61	0.2222	0.3649	0.5956	0.61	0.2248	0.3688	0.5961
0.74	0.1754	0.2947	0.7007	0.67	0.1978	0.3241	0.6471	0.65	0.2072	0.3472	0.6157	0.65	0.2064	0.3458	0.6170
0.77	0.1584	0.2736	0.7122	0.72	0.1748	0.2960	0.6731	0.68	0.1924	0.3294	0.6333	0.68	0.1883	0.3229	0.6334
0.8	0.1416	0.2528	0.7178	0.78	0.1440	0.2571	0.6974	0.71	0.1774	0.3098	0.6516	0.72	0.1719	0.3019	0.6494
0.84	0.1236	0.2288	0.7226	0.85	0.1133	0.2152	0.7113	0.75	0.1627	0.2914	0.6651	0.75	0.1551	0.2817	0.6573
0.87	0.1067	0.2059	0.7211	0.92	0.0799	0.1672	0.6977	0.78	0.1468	0.2707	0.6747	0.78	0.1370	0.2601	0.6569
0.91	0.0904	0.1827	0.7142	0.99	0.0371	0.1019	0.5714	0.81	0.1326	0.2520	0.6823	0.82	0.1208	0.2385	0.6585
0.97	0.0515	0.1238	0.6446	1.05	-0.0319	-0.0077	-0.9483	0.85	0.1178	0.2318	0.6864	0.85	0.1045	0.2165	0.6533
1.01	0.0264	0.0849	0.4975	1.12	-0.0568	-0.0067	-1.1330	0.88	0.1015	0.2090	0.6824	0.88	0.0879	0.1934	0.6392
1.04	-0.0126	0.0225	-0.9279					0.92	0.0850	0.1846	0.6712	0.92	0.0717	0.1718	0.6093
								0.95	0.0661	0.1560	0.6397	0.95	0.0539	0.1467	0.5558
								0.98	0.0442	0.1230	0.5616	0.98	0.0355	0.1201	0.4628
								1.02	0.0122	0.0739	0.2683	1.02	0.0152	0.0888	0.2773
								1.05	-0.0301	0.0047	-10.7200	1.05	-0.0173	0.0381	-0.7620

At Cavitation Number=3.08

J	KT	10KQ	Eta												
---	----	------	-----	---	----	------	-----	---	----	------	-----	---	----	------	-----

0.53	0.2749	0.4233	0.5438	0.52	0.2582	0.4023	0.5302	0.5	0.2695	0.4279	0.5016	0.5	0.2703	0.4321	0.4979
0.51	0.2824	0.4326	0.5312	0.61	0.2163	0.3504	0.6041	0.58	0.2362	0.3862	0.5620	0.58	0.2427	0.3871	0.5793
0.6	0.2383	0.3780	0.6056	0.65	0.2007	0.3314	0.6262	0.62	0.2189	0.3653	0.5867	0.61	0.2247	0.3635	0.6047
0.64	0.2203	0.3561	0.6306	0.68	0.1857	0.3130	0.6451	0.65	0.2041	0.3478	0.6057	0.65	0.2064	0.3404	0.6263
0.67	0.2037	0.3350	0.6522	0.72	0.1702	0.2936	0.6617	0.68	0.1891	0.3300	0.6217	0.68	0.1899	0.3202	0.6422
0.71	0.1876	0.3150	0.6694	0.75	0.1558	0.2755	0.6752	0.71	0.1742	0.3110	0.6372	0.72	0.1708	0.2981	0.6524
0.74	0.1720	0.2954	0.6854	0.78	0.1401	0.2542	0.6879	0.75	0.1599	0.2921	0.6519	0.75	0.1535	0.2775	0.6607
0.77	0.1546	0.2727	0.6976	0.82	0.1259	0.2345	0.6977	0.79	0.1417	0.2678	0.6653	0.79	0.1315	0.2496	0.6648
0.81	0.1382	0.2516	0.7056	0.85	0.1104	0.2133	0.7018	0.83	0.1241	0.2437	0.6755	0.83	0.1104	0.2218	0.6614
0.84	0.1217	0.2300	0.7083	0.88	0.0961	0.1938	0.6975	0.87	0.1066	0.2196	0.6742	0.88	0.0885	0.1928	0.6405
0.87	0.1058	0.2078	0.7081	0.92	0.0809	0.1729	0.6828	0.91	0.0881	0.1939	0.6616	0.92	0.0687	0.1660	0.6042
0.91	0.0890	0.1853	0.6936	0.95	0.0648	0.1508	0.6486	0.96	0.0674	0.1652	0.6206	0.96	0.0464	0.1350	0.5248
0.97	0.0534	0.1350	0.6131	0.98	0.0463	0.1249	0.5806					1	0.0249	0.1043	0.3815
1.01	0.0338	0.1067	0.5075												
1.04	0.0133	0.0756	0.2909												
1.11	-0.0330	0.0050	-11.7222												

At Cavitation Number=4.56

J	KT	10KQ	Eta	J	KT	10KQ	Eta	J	KT	10KQ	Eta	J	KT	10KQ	Eta
0.53	0.2684	0.4251	0.5319	0.52	0.2543	0.4039	0.5203	0.52	0.2543	0.4039	0.5203	0.52	0.2624	0.4229	0.5171
0.56	0.2523	0.4052	0.5579	0.58	0.2273	0.3681	0.5737	0.58	0.2273	0.3681	0.5737	0.57	0.2380	0.3939	0.5528
0.61	0.2318	0.3803	0.5879	0.62	0.2113	0.3483	0.5949	0.62	0.2113	0.3483	0.5949	0.61	0.2188	0.3705	0.5758
0.64	0.2144	0.3582	0.6107	0.65	0.1966	0.3290	0.6174	0.65	0.1966	0.3290	0.6174	0.65	0.2003	0.3483	0.5932
0.68	0.1984	0.3373	0.6318	0.68	0.1818	0.3121	0.6332	0.68	0.1818	0.3121	0.6332	0.68	0.1829	0.3268	0.6084
0.71	0.1824	0.3175	0.6467	0.72	0.1674	0.2944	0.6475	0.72	0.1674	0.2944	0.6475	0.72	0.1654	0.3052	0.6189
0.74	0.1671	0.2979	0.6616	0.75	0.1519	0.2733	0.6651	0.75	0.1519	0.2733	0.6651	0.75	0.1492	0.2841	0.6279
0.77	0.1510	0.2772	0.6704	0.78	0.1377	0.2534	0.6773	0.78	0.1377	0.2534	0.6773	0.79	0.1319	0.2629	0.6269
0.81	0.1341	0.2550	0.6764	0.82	0.1227	0.2336	0.6835	0.82	0.1227	0.2336	0.6835	0.82	0.1162	0.2426	0.6234
0.84	0.1185	0.2341	0.6766	0.85	0.1080	0.2134	0.6857	0.85	0.1080	0.2134	0.6857	0.85	0.0999	0.2211	0.6113
0.87	0.1017	0.2104	0.6726	0.88	0.0940	0.1913	0.6913	0.88	0.0940	0.1913	0.6913	0.89	0.0826	0.1971	0.5907
0.9	0.0870	0.1896	0.6607	0.92	0.0793	0.1709	0.6765	0.92	0.0793	0.1709	0.6765	0.92	0.0666	0.1752	0.5560
0.94	0.0687	0.1648	0.6236	0.95	0.0633	0.1482	0.6462	0.95	0.0633	0.1482	0.6462	0.95	0.0494	0.1513	0.4943
0.97	0.0518	0.1419	0.5641	0.98	0.0467	0.1279	0.5712	0.98	0.0467	0.1279	0.5712	0.99	0.0323	0.1264	0.4015
1.01	0.0314	0.1138	0.4424									1.02	0.0172	0.1042	0.2661
1.04	0.0120	0.0862	0.2310									1.05	-0.0020	0.0750	-0.0440
1.11	-0.0296	0.0253	-2.0592									1.08	-0.0217	0.0460	-0.8142
												1.12	-0.0432	0.0154	-4.9874